https://ntrs.nasa.gov/search.jsp?R=20140006956 2019-06-29T12:27:41+00:00Z

Astroparticle Physics 45 (2013) 56–70

Contents lists available at SciVerse ScienceDirect

Astroparticle Physics

journal homepage: www.elsevier.com/locate/astropart

The Astrophysical Multimessenger Observatory Network (AMON)

M.W.E. Smith [a,b,*], D.B. Fox [c,b], D.F. Cowen [a,c,b], P. Mészáros [a,c,b], G. Tešić [a,b], J. Fixelle [c], I. Bartos [d], P. Sommers [a,c,b], Abhay Ashtekar [a,b], G. Jogesh Babu [e,c], S.D. Barthelmy [f], S. Coutu [a,b], T. DeYoung [a,b], A.D. Falcone [c,b], Shan Gao [a,b], B. Hashemi [a], A. Homeier [g], S. Márka [d], B.J. Owen [a,b], I. Taboada [h]

[a] Department of Physics, Pennsylvania State University, University Park, PA 16802, USA
[b] Institute for Gravitation and the Cosmos, Pennsylvania State University, University Park, PA 16802, USA
[c] Department of Astronomy & Astrophysics, Pennsylvania State University, University Park, PA 16802, USA
[d] Department of Physics & Columbia Astrophysics Laboratory, Columbia University, New York, NY 10027, USA
[e] Department of Statistics, Pennsylvania State University, University Park, PA 16802, USA
[f] NASA Goddard Space Flight Center, Code 661, Greenbelt, MD 20771, USA
[g] Physikalisches Institut, Universität Bonn, Nussallee 12, D-53115 Bonn, Germany
[h] Center for Relativistic Astrophysics, School of Physics, Georgia Institute of Technology, Atlanta, GA 30332, USA

ARTICLE INFO

Article history:
Received 3 December 2012
Received in revised form 1 February 2013
Accepted 15 March 2013
Available online 28 March 2013

Keywords:
High-energy astrophysics
Gravitational radiation
Neutrinos
Cosmic rays
Gamma-ray bursts
Supernovae

ABSTRACT

We summarize the science opportunity, design elements, current and projected partner observatories, and anticipated science returns of the Astrophysical Multimessenger Observatory Network (AMON). AMON will link multiple current and future high-energy, multimessenger, and follow-up observatories together into a single network, enabling near real-time coincidence searches for multimessenger astrophysical transients and their electromagnetic counterparts. Candidate and high-confidence multimessenger transient events will be identified, characterized, and distributed as AMON alerts within the network and to interested external observers, leading to follow-up observations across the electromagnetic spectrum. In this way, AMON aims to evoke the discovery of multimessenger transients from within observatory subthreshold data streams and facilitate the exploitation of these transients for purposes of astronomy and fundamental physics. As a central hub of global multimessenger science, AMON will also enable cross-collaboration analyses of archival datasets in search of rare or exotic astrophysical phenomena.

© 2013 Elsevier B.V. All rights reserved.

1. Introduction

We stand at the dawn of multimessenger astrophysics – a quest to use the messenger particles of all four of nature's fundamental forces to explore the most violent phenomena in the universe. Observatories first imagined a generation ago are finally being realized, including the Advanced LIGO [1] and Virgo [2] gravitational-wave detectors, the ANTARES [3] and IceCube [4] high-energy neutrino observatories, and the Pierre Auger Cosmic Ray Observatory [5]. On the ground and in space, they are complemented by high-energy observatories including the Swift [6] and Fermi [7] satellites, the HESS [8], VERITAS [9], and MAGIC [10] TeV gamma-ray telescopes, and the HAWC [11] TeV gamma-ray observatory.

Collectively, these facilities promise the first detections of gravitational waves and high-energy cosmic neutrinos, the resolution of the mystery surrounding the origins of ultrahigh-energy cosmic rays, and a new window into the formation and evolution of black holes. Given their nature as first-generation facilities, however, the sensitivities of the non-electromagnetic observatories are naturally limited, with rates of detection for transient events of publishable significance known or expected to be low, perhaps a handful per year (or, in the case of Advanced LIGO and Virgo at design sensitivity, a few dozen [1]).

During the intervals prior to and between detection of these rare high-significance events, the multimessenger facilities will be buffeted by signals from a far greater number of lower-significance events that will be statistically indistinguishable from background or noise processes. Such "subthreshold" events are, by definition, unrecoverable as astrophysical signals in the data

* Corresponding author at: Department of Physics, Pennsylvania State University, University Park, PA 16802, USA. Tel.: +1 814 380 1763.
E-mail addresses: msmith@gravity.psu.edu (M.W.E. Smith), dfox@astro.psu.edu (D.B. Fox), cowen@phys.psu.edu (D.F. Cowen), nnp@astro.psu.edu (P. Mészáros), gut10@psu.edu (G. Tešić), jxf5078@psu.edu (J. Fixelle), ibartos@phys.columbia.edu (I. Bartos), sommers@phys.psu.edu (P. Sommers), ashtekar@gravity.psu.edu (A. Ashtekar), babu@psu.edu (G. Jogesh Babu), scott.d.barthelmy@nasa.gov (S.D. Barthelmy), coutu@phys.psu.edu (S. Coutu), deyoung@phys.psu.edu (T. DeYoung), afalcone@astro.psu.edu (A.D. Falcone), sxg324@psu.edu (S. Gao), bth5032@psu.edu (B. Hashemi), homeier@physik.uni-bonn.de (A. Homeier), sm2375@columbia.edu (S. Márka), owen@gravity.psu.edu (B.J. Owen), itaboada@gatech.edu (I. Taboada).

0927-6505/$ - see front matter © 2013 Elsevier B.V. All rights reserved.
http://dx.doi.org/10.1016/j.astropartphys.2013.03.003

stream of any individual facility. However, if they are accompanied by a subthreshold signal in another multimessenger channel they can be identified, and potentially achieve high significance, via careful coincidence analysis of the data streams from multiple facilities.

In this paper we present the scientific case for the Astrophysical Multimessenger Observatory Network and describe its important elements. AMON will weave together existing and forthcoming high-energy astrophysical observatories into a single virtual system, capable of sifting through the various data streams in near real-time, identifying candidate and high-significance multimessenger transient events, and providing alerts to interested observers.

As we show, AMON will enable a significant enhancement in the effective aggregate sensitivity of the world's leading multimessenger facilities for a small fraction of the facilities' total cost, provide the first near real-time alerts for multimessenger transient sources, and simplify the mechanics and politics of cross-collaboration analyses for all partners. As such, we believe AMON represents a natural next step in the extension of the global astronomical community's vision beyond the electromagnetic (EM) spectrum.

The development of AMON is currently underway. Signatories to the AMON Memorandum of Understanding[1] (MOU) include the IceCube and ANTARES neutrino observatories, the VERITAS and HAWC TeV γ-ray observatories, and the Swift orbital telescope. Exploratory discussions with the LIGO (including GEO-600), and Fermi scientific collaborations have led to signed letters of commitment, with negotiations toward MOU signatures from all parties ongoing. Discussions have also been initiated with candidate follow-up facilities including ROTSE-III [12] and the Palomar Transient Factory [13], with the goal of bringing these observatories into the collaboration prior to or shortly after the commencement of real-time AMON alert operations.

AMON is structured as an open and extensible network, with an MOU that allows straightforward incorporation of new triggering and follow-up facilities. Collaborations interested in the scientific goals of AMON, and with useful triggering or follow-up capabilities to contribute, are encouraged to contact the authors for information about joining AMON. First versions of the necessary supporting hardware and software infrastructure for AMON are being installed at Penn State, and initial analyses on archival and simulated real-time data streams will get under way shortly thereafter, as a means of preparing to bring the first set of triggering facilities on-line within the next year.

The paper is structured as follows: In Section 2 we provide an overview of the scientific opportunity for AMON which motivates our efforts. In Section 3 we discuss the elements of AMON, including the technical and operational protocols that we propose to adopt in linking the partner facilities, and the algorithms that we will use to identify coincident signals. Section 4 presents detailed simulations of multimessenger transient sources, and additional theoretical case studies, which illustrate the gains that stand to be realized by AMON. Section 5 presents our summary and conclusions.

2. The AMON science opportunity

AMON is intended to contribute in several ways to the first decade of multimessenger astronomy. A common focus of these approaches is on multimessenger transient events that are observed as coincident (potentially subthreshold) signals in the data of AMON partner facilities corresponding to two or more distinct types of messenger particle. In this section, we briefly review the strongest candidates for these multimessenger transient sources and the current theoretical expectations for their properties, rates, and broader implications for physics and astrophysics.

2.1. High-luminosity gamma-ray bursts

As the most violent cataclysms known, and as the sites of the most highly-relativistic cosmic outflows, gamma-ray bursts (GRBs) have long been considered likely multimessenger transient sources. Recent progress in distinguishing the distances and energetics of GRBs and understanding the likely nature of their progenitors [14] means that we can review the expected multimessenger signals of the different varieties of GRB on a case by case basis.

The traditional or "classical" long-duration, high-luminosity gamma-ray bursts (HL-GRBs) are the most common type of GRB detected by satellite experiments, being observed as bright seconds- to minutes-long bursts of γ-radiation from high-redshift, $z \gtrsim 1$. HL-GRBs are believed to arise when a massive star ($M \gtrsim 25 M_\odot$) undergoes core collapse to a black hole (BH); confirmation of this "collapsar" model [15] for the HL-GRBs has been most dramatically provided by spectroscopic observations of ensuing type Ibc supernovae (SNe), with other lines of evidence also contributing [16].

In the collapsar model, formation of a high angular-momentum BH and accretion of residual gas through an accretion disk produces a relativistic jet. In "successful" GRBs the jet pierces the stellar envelope, accelerates to high Lorentz factor, and radiates gamma-rays for tens of seconds, providing a bright electromagnetic trigger for observers within the jet collimation angle. The typical HL-GRB jet energy of $E \sim 10^{51}$–10^{52} erg, collimated within an angle of $\langle\theta\rangle \sim 5^\circ$, roughly 1/250 of the sky, yields the observed isotropic-equivalent energies of $E_0 = E(4\pi/\Omega_j) \sim 10^{53}$–$10^{54}$ erg [17]. For a burst duration $T \sim 10$ s, this corresponds to an isotropic-equivalent luminosity $L_\gamma \sim E_0/T = 10^{52}$–$10^{53}$ erg s^{-1}. Given a 250:1 jet collimation factor, the nearest off-axis bursts are anticipated to be located $250^{1/3} \sim 6$ times closer than the nearest on-axis bursts. Off-axis bursts, defined as bursts whose bright initial γ-ray emission does not illuminate observers at Earth, may still be observed via their less luminous shock-breakout emission, their prompt gravitational wave (GW) signal, or their subsequent afterglow and/or supernova components.

In the standard internal-shock model, the gamma-ray emission of HL-GRBs is produced by internal shocks at a dissipation radius $r_d \sim \Gamma^2 c\,\delta t \sim (3\times 10^{13}\ \mathrm{cm})\,\eta_{2.5}^2\,\delta t_{-2}$ [18], where $\eta_{2.5} = \Gamma/300$ is the bulk Lorentz factor divided by 300 and $\delta t_{-2} = \delta t/10^{-2}$ s is the variability time of the central engine in hundredths of a second. These shocks Fermi-accelerate electrons, which produce gamma-rays via synchrotron and inverse Compton scattering, and are then boosted by the bulk motion of the relativistic outflow. For a discussion of alternative models see Ref. [19].

The same shocks responsible for electron acceleration and γ-ray emission should also accelerate protons, leading to photo-produced pions which in turn yield high-energy cosmic neutrinos (CN) and γ-rays from charged and neutral pion decays, respectively [20,21]. Initial assumptions were that the energy in relativistic protons would be of the same order as the energy emitted in γ-rays, $E_p \simeq (1/f_e)E_\gamma$, where $f_e \lesssim 1$ is the fraction of proton energy given to electrons (and observed as GRB photons), so that the optical depth $\tau_{p\gamma}$ determines the CN and TeV gamma-ray luminosity, $L_{\mathrm{TeV}} \sim \tau_{p\gamma} L_p$. The CN to γ-ray flux ratio expected in this model has been quantified [22] and used by IceCube [23–25] to set limits which are already a factor of five below the naive predictions. However, careful consideration of the underlying physics [26–28] suggests that IceCube observations will need to continue for several more years before the somewhat reduced CN fluxes of more

[1] The AMON MOU is available at http://amon.gravity.psu.edu/mou.shtml.

realistic models are tested. Ultimately, detection of GRB-related CN is expected if HL-GRBs contribute a significant fraction of the highest-energy cosmic rays.

Regardless of the total energy release of the HL-GRBs, which may well be an order of magnitude or more above the beaming-corrected γ-ray energies $E \lesssim 10^{52}$ erg, no significant GW emission will be produced if the core collapse, jet production, and burst processes maintain approximate axisymmetry throughout. However, it is possible for a rapidly rotating core and accretion disk to develop bar and/or fragmentation instabilities which could result in substantial GW emission. In the most optimistic case [29] the resulting GW signal is periodic and roughly as strong as the signal from neutron star binary mergers, and hence, visible out to similar distances (hundreds of Mpc for the advanced facilities) using ground-based GW detectors.

While some 3D simulations of stellar collapse suggest a fragmentary process, and a correspondingly weaker GW energy release $E_{GW} \sim 10^{-7} M_{\odot} c^2 \sim 10^{47}$ erg [30], these have not included relativistic effects that are known to contribute to large bar asymmetries [31], as manifested in other simulations [32]. When present, these instabilities result in GW emission comparable to that found in optimistic analytical calculations [29].

2.2. Low-luminosity gamma-ray bursts

Low-luminosity GRBs (LL-GRBs) are underluminous long-duration GRBs, having substantially lower isotropic-equivalent energies, $E_0 \sim 10^{49}$–10^{50} erg, than the HL-GRBs. Because of their lower γ-luminosities, they are currently only detected at low redshift, $z \lesssim 0.5$, where they provide the bulk of the observed GRB-SN Ibc associations [16]. Estimates of the LL-GRB rate suggest that they occur at $\gtrsim 100$ times the rate of HL-GRBs while constituting $\lesssim 1\%$ the rate of type Ibc SNe overall [33–36].

The γ-ray emission of LL-GRBs may be due, in some or all cases, to a relativistic shock breakout [37,38] and hence may not require the Lorentz factor $\Gamma \gtrsim 100$ jet needed to explain the high-luminosity, high-variability γ-emission of HL-GRBs. Such shock breakout emission would also be expected to be uncollimated (uniform over the sky) or nearly so.

Predictions for the CN emissions of LL-GRBs have been explored by Murase et al. [39] and Gupta and Zhang [40] for relativistic jet models and by Kashiyama et al. [41] for shock breakout models. In relativistic jet models, a straightforward approach scales CN fluxes from HL-GRB predictions according to their γ-ray luminosities, and anticipates similar spectra with $E_\nu^2 \phi_\nu$ peaking at PeV–EeV energies. Given current evidence for less-relativistic jets in LL-GRBs, however, these predictions may be optimistic.

Shock breakout models [41], by contrast, predict softer neutrino spectra peaking in the TeV–PeV range, with luminosities for reference events that would make individual bursts detectable to IceCube within a horizon of $D \lesssim 10$ Mpc. The LL-GRB rate within this horizon is thought to be small, $r \sim 0.002\ \mathrm{yr}^{-1}$, but prospects for detection could be improved by stacking analyses using $\sim$dozens of more distant events identified by their prompt high-energy EM signature.

Similarities in explosion energy, ejecta velocity, and synthesized nickel mass for the type Ibc supernovae of LL-GRB and HL-GRB events suggest that the details of core collapse for the two event classes, and their GW emissions, may be similar. However, given the critical role that high values of core angular momentum are thought to play in powering HL-GRB jets, and the need for accretion or disk instabilities to power significant GW emission, the relative weakness of LL-GRB jets may suggest correspondingly reduced prospects for GW emission. If the GW emissions are competitive with those of binary neutron star–neutron star (NS–NS) mergers in even some cases, this would make the LL-GRBs with their relatively isotropic γ-ray emissions a highly-promising target population for ground-based GW detectors.

2.3. Short-hard gamma-ray bursts

Short-hard gamma-ray bursts (SHBs), apart from their shorter durations and somewhat harder spectra, are observationally similar to HL-GRBs. Their harder spectra may indicate higher bulk Lorentz factors [18], while their reduced durations, $t_b \lesssim 2$ s, suggest shorter accretion timescales compared to those of the HL-GRB collapsars. A softer "extended emission" episode lasting for $t \sim 30$–100 s after the burst itself is present in about a third of SHBs, accounting for 5–20% of the total energy [42].

Thanks to afterglow discoveries and host galaxy identifications of the Swift era, consensus now holds that SHBs are likely due to compact binary (NS–NS or NS–BH) mergers [43,14]. If so, these events are associated with progenitor systems that are observed within our own Galaxy (as relativistic NS–NS pulsar binaries), have merger rates that can be estimated from population synthesis modeling (e.g. [44]), and should emit strong GW emission in a highly-calculable "chirp" waveform across the frequency range of ground-based GW observatories just prior to merger. Indeed, binary mergers are the primary extragalactic target population for next-generation LIGO and VIRGO, with expected event rates at full design sensitivity expected to reach dozens annually [1].

Afterglow observations for a handful of Swift-detected SHBs show evidence for typical collimation angles $\langle\theta\rangle \gtrsim 6^\circ$, corresponding to beaming fractions of 200:1 (similar to that for HL-GRBs) or less [45]. These beaming corrections adjust the observed isotropic-equivalent energies of the bursts, $E_0 \gtrsim 10^{51}$ erg to lower inferred jet energies $E \sim 10^{48}$–10^{50} erg. As such the nearest off-axis mergers are predicted to be observed at $200^{1/3} \sim 6$ times closer distance than the nearest on-axis events, where they may be detected as GW inspiral signals without SHB counterparts.

Because of their very similar γ-ray characteristics and inferred jet properties, it is assumed that the radiation physics of the HL-GRBs and SHBs are similar, apart from possible slight differences due to the SHBs' reduced durations and potentially larger Lorentz factors and collimation angles [18]. CN production models may thus conservatively be carried forward by assuming similar CN to γ-ray flux ratios as for the HL-GRBs.

In terms of GW emission, SHBs in the compact binary merger model represent a "dream scenario", as systems in which the GW waveform is known to be strong (detectable to hundreds of Mpc by advanced detectors) and calculable, and moreover, has already been implemented in data analysis systems via matched-filter algorithms that will be run in real-time by LIGO and VIRGO, enabling the observatories to distribute GW "inspiral alerts" to interested observers. The primary questions for the near future, then, are whether the GW inspiral signatures of these mergers will be detected, at what rate, and whether or not a coincident γ-ray or other electromagnetic signature can be identified. Unless our understanding is rather radically misplaced, all three questions are likely to be resolved once the era of the advanced GW facilities is fully under way.

2.4. Choked jet supernovae

The choked jet supernova, a theoretical scenario, represents the alternative fate that awaits a massive star if its core collapse generates a high-energy jet as in HL-GRBs, but in a fashion or within the context of a higher-mass stellar envelope that absorbs the jet energy before it is able to escape the star. As such, the choked-jet events evince no high-luminosity γ-ray emission; however, in the course of being quenched, their sub-stellar jets may undergo internal shocks which could accelerate protons and yield $p\gamma$ and pp

neutrinos in the TeV range [46–48]. Observationally, then, the choked-jet supernovae would be observed as a relatively low-redshift, highly-energetic supernova (a hypernova) with associated CN emission.

Event rate estimates for choked-jet events are necessarily speculative. However, we note that if the process that leads to high-energy jet production during core collapse is largely independent of the nature of the overlying stellar envelope, then the choked-jet supernova rate may be comparable to the rate of HL-GRBs. Moreover, given that the collapsar mechanism has multiple failure modes, including a high-mass stellar envelope, insufficient rotation, and too much jet precession [49], one can speculate that choked jet supernovae should, on generic grounds, be more common than HL-GRBs, although potentially (for these and related reasons) exhibiting less-luminous CN and/or GW emission.

2.5. Core collapse supernovae

Core-collapse supernovae (CCSNe) are expected roughly every 30–100 yr in our Galaxy; given the direct heritage of the revolutionary neutrino detection of SN 1987A [50], any such Galactic cataclysm would obviously represent a first-grade candidate multimessenger transient.

Seen in relatively nearby galaxies (distances $D \lesssim 100$ Mpc), CCSNe are typically detected by optical observers within a few days, although as Swift has demonstrated [51], prompt detection of the high-energy shock breakout can be realized with sufficiently sensitive instrumentation. On this timescale, the prompt thermal ($E_\nu \gtrsim 10$ MeV) neutrinos should be detectable by IceCube and Super-Kamiokande for events within $D \lesssim 50$ kpc [52].

CN may be produced by these "ordinary" CCSNe, either at shock breakout [41] or at later times, via interaction of the SN shockwave with a dense circumstellar medium [53]. The shock breakout CN emissions of ordinary CCSNe will be fainter than for the LL-GRBs, and so require very nearby events or larger-scale stacking analyses to detect with IceCube. CCSNe circumstellar interactions have the potential to generate a greater number of CN over an extended timescale of weeks to months, and may be detectable with IceCube, if candidate CN CCSNe can be identified with confidence and in sufficient numbers to make a sensitive search.

GW emission from generic CCSNe are expected to be relatively weak [54], and hence, not detectable except in the case of a Galactic (or possibly, Small or Large Magellanic Cloud) event.

Cosmic rays with energies below the "ankle" of the spectrum at $E \approx 4 \times 10^{18}$ eV are generally attributed to sources within the Galaxy [55]. Since no steady sources have been detected despite sensitive searches [56], they may be produced in occasional bursts within the Galaxy, including Galactic CCSNe. The decay length for relativistic neutrons is $9.2\,E_{18}$ kpc, where E_{18} is the neutron energy in EeV. Transient sources of neutrons of 1 EeV or above can thus be detected across much of the Galactic disk, including the central bulge region, and at higher energies also accessible with Auger, sources throughout most of the halo are detectable.

2.6. Blazars

Blazars are frequently detected in γ-rays at GeV (Fermi, AGILE) and TeV (HESS, VERITAS, MAGIC) energies; they are also highly luminous X-ray, optical, and radio sources. Since the non-thermal X-ray emission of blazars is generally understood to be synchrotron emission from electrons accelerated in shocks of an inner jet, shock-accelerated protons are expected as well. The target photons for $p\gamma$ interactions, leading to CN emission, could then be either synchrotron photons from co-accelerated electrons, or optical/UV photons originating in the accretion disk or scattered into the jet by broad-line region clouds.

Blazars are highly variable, flaring sources that are much brighter across the EM spectrum during flare episodes than in quiescence. Expected CN fluxes for standard blazar models [21,57,58] suggest that typical individual flares cannot be detected with IceCube, with the summed contribution of $\gtrsim 100$ such flares required to yield an expected >1 CN detection in IceCube. Separately, limits on the diffuse CN flux due to the summed contribution of all blazars in the Northern hemisphere have been published by IceCube using the 40-string (roughly one year integration) dataset, constraining some models [24], but without the statistical leverage that would be provided by comprehensive EM monitoring yielding the times and durations of blazar flares.

Individual spectral components of blazar flares are also variable, and the properties of the highest-energy components are poorly constrained due to the difficulty in obtaining sensitive TeV γ-ray data and simultaneous flare-triggered multiwavelength EM coverage. Moreover, recent Fermi and multiwavelength data suggest that spectral breaks and possible additional components are present during some blazar emission episodes [59–61]. Exceptional TeV γ-ray flares from blazars that lack associated X-ray emission, analogs of the 1ES 1959+650 "orphan" TeV flare [62–64], could be associated with hadron acceleration that would yield CN fluxes well in excess of those expected from typical flares, and hence, would be more readily detected by current facilities.

Energetic GW emission from blazars in the frequency range of ground-based detectors is not anticipated.

2.7. Primordial black holes and other exotica

If primordial black holes (PBHs) formed in the early universe with masses $M \sim 5 \times 10^{14}$ g appropriate for them to undergo explosive evaporation at the present epoch [65], then they would serve as a distinct and exotic type of multimessenger transient.

As the black hole loses mass via Hawking radiation, $dM/dt = -\alpha(M)/G^2M^2$ [66], its temperature $T_{\rm BH}$ increases, allowing an increasing number of particle types (degrees of freedom or *dof*) $\alpha(M)$ to be radiated. Once $T_{\rm BH}$ reaches the quantum chromodynamic energy scale of $\Lambda_{\rm QCD} \gtrsim 200$ MeV, free quarks and gluons will be emitted and fragment into hadrons, photons and leptons, resulting in a flux of high-energy cosmic ray neutrons and CN [67] that might be detectable from Auger and IceCube.

Detection of PBHs would give dramatic confirmation of Hawking's hypothesis and theories positing early cosmological phase transitions (e.g. [68,69]), and enable studies that would likely yield deep insights into ultrahigh-energy physics as well as quantum gravity.

Other primordial relics, if they exist, might have decay modes yielding harder spectra than the PBHs (e.g. [70–76]). Power-law spectra with $n \propto E^{-2}$ or harder would put out a majority of the total decay energy at the highest energies, meaning that the first detections, or most sensitive limits, on these processes are likely to arise from the highest-energy (largest area) facilities, IceCube and Pierre Auger.

3. AMON dataflow and operations

Multimessenger detection of one of the astrophysical sources described above, or of some entirely distinct cosmic phenomenon, will require coordination and cooperation between observatories of strikingly different design and operation. These observatories produce data whose heterogeneity motivates the unified approach of AMON for detecting coincidences. Individual facilities participating in AMON can be characterized as triggering facilities, follow-up facilities, or both. Triggering facilities are typically sensitive to one or more messenger type (photons, cosmic rays, neutrinos, or

Table 1
(a) False Positive Rate (FPR) in units of yr^{-1} for single event streams, including *above threshold* events that can lead to stand-alone discoveries and the background-dominated *subthreshold* events that are transmitted to AMON. (b) A coarse clustering analysis, shown here for a 3σ spatial window and $\Delta T = 100$ s, will primarily identify pairs of coincident subthreshold events with corresponding pairwise FPR. This FPR can be further reduced with a likelihood analysis to tune the distribution rate of AMON Alerts, with the subsequent discovery of EM afterglow proving definitive. (c) If three or more subthreshold events are detected by the clustering analysis (shown here for all possible combinations that include at least one event from a given stream), or if some other constraint is applied, the FPR is reduced to a level that enables a definitive or near-definitive claim of discovery.

		IceCube	ANTARES	LIGO-Virgo	Auger	BAT	GBM	LAT	HAWC
(a) Single streams	Above thresh.	~0	~0	~0	~0	~100	~250	~10	~10
	Subthreshold	8.8×10^4	2.9×10^4	3.2×10^3	2.4×10^5	1.4×10^5	3.1×10^2	3.9×10^4	2.6×10^4
	IceCube	30	1.5	35	1.8	11	10	24	6.5
	ANTARES	1.5	0.5	12	1.1	0.7	3.5	7.1	0.6
	LIGO-Virgo	35	12	N/A	8.4	53	0.6	16	10
(b) Pairwise FPR	Auger[a]	1.8	1.1	8.4	20	2.9	2.5	5.9	1.5
	BAT	11	0.7	53	2.9	N/A	16	32	3.3
	GBM	10	3.5	0.6	2.5	16	N/A	5.0	3.2
	LAT	24	7.1	16	5.9	32	5.0	N/A	6.8
	HAWC	6.5	0.6	10	1.5	3.3	3.2	6.8	N/A
	GRB lt. curve[b]	0.071	0.003	0.16	–	0.0004	0.08	0.13	0.019
	SNe lt. curve[b]	1.5	0.07	3.4	–	0.009	1.6	2.7	0.4
(c) High significance	3-fold coinc.	0.15	0.03	0.31	0.64	0.12	0.09	0.40	0.08
	3-fold coinc[a]	0.10	0.02	0.15	0.06	0.08	0.04	0.23	0.04
	High-sig. EM[c]	0.015	0.002	0.045	0.044	0.010	0.014	0.039	0.005
	PBH search[d]	0.13	0.01	–	0.21	–	–	–	0.35

[a] Auger events for the pairwise (and optionally threefold) analysis are selected with galactic latitude within $\pm 5^\circ$ and energy $\geqslant 1$ EeV.
[b] Coincidence rate of event pairs with serendipitous follow-up detection of a GRB or SNe light curve (not including galactic searches).
[c] Event pairs with above threshold EM detection. GBM not included as the high significance partner, due to poor spatial localization.
[d] An additional temporal cut of $\Delta T = 1$ s is applied to the pairwise analysis for TeV and higher observatories, to search for primordial black holes and other exotic phenomena. Shown here are the FPRs for pairwise coincidences with HAWC.

gravitational waves) and search in a wide field of view or monitor known sources for transient behavior. From their raw data, they construct candidate astrophysical events, here denoted "trigger events", which may transmitted through either public or private channels to AMON. These variously represent a single particle interaction (e.g., a muon neutrino interaction detected by IceCube), multiple detections processed into a high level trigger (e.g., a Swift BAT light curve), or a sharp rise in a continuous measurement (e.g., an Advanced LIGO event).

For AMON, a fundamental characterization of each observatory is its event-wise false positive rate (FPR). The FPR is the dominant component of the total event rate that each observatory sends to AMON. The FPR is typically due to intrinsic detector noise or irreducible backgrounds that produce signal-like events. The FPRs for all triggering observatories considered here are listed in Table 1a. Later in this section we describe how these FPRs are calculated.

By design, AMON will handle data streams dominated by these subthreshold signal-like events that individually cannot rise to the level of astrophysical discovery. For example, a single muon neutrino detected by IceCube could be of astrophysical origin, but the channel is indistinguishable from, and dominated by, atmospheric muon neutrinos. Similarly, single Galactic neutrons in Auger cannot be distinguished from the dominant background of charged particle cosmic ray events, and lowering the threshold of X-ray, γ-ray, or gravitational wave detectors increases signal acceptance at the cost of simultaneously admitting many additional accidental noise events. However, if two or more of these events are correlated in arrival direction and time they can attain a combined significance that results in AMON issuing an "Alert." An Alert either constitutes an immediate discovery or prompts follow-up observations that could demonstrate the presence of a "smoking gun" electromagnetic counterpart. By having all individual observatory FPRs on hand, algorithms running in the AMON framework are uniquely capable of calculating the aggregate Alert FPR associated with each coincidence detection. The Alert FPR is a statistical measure of the quality of a given multimessenger coincidence, endowing each Alert with a high degree of utility for multimessenger source searches.

It is also possible for trigger events from a single observatory to be intrinsically above threshold, allowing the observatory to make a stand-alone claim for discovery. A burst of three neutrinos in close directional and temporal coincidence (IceCube or ANTARES), a burst of three air showers in coincidence (Auger), especially if their putative source is close enough for them to be neutrons, a statistically significant burst of hard X-rays (Swift BAT, Fermi GBM) or γ-rays (Fermi LAT or HAWC), or a strong strain registered by a gravitational wave detector (LIGO-Virgo) would each constitute a discovery. For these stand-alone discoveries, AMON can serve as a quick and convenient conduit for disseminating the source coordinates, enabling timely follow-up observations at multiple disparate observatories. AMON will leverage the GRB Coordinates Network (GCN) [77], among others, to promulgate its Alerts.

Underpinning AMON's sensitivity to new phenomena is the broad (multiple steradian) sky coverage and high duty cycles of the triggering observatories. Fig. 1 shows the results of a simulation of a calendar year for the triggering facilities that have signed the AMON MOU (IceCube, ANTARES, Auger, HAWC, and Swift BAT) and potential future signatories (Fermi LAT and GBM, and LIGO-Virgo), establishing that – absent severe disruptions – at least two facilities are always observing any given part of the sky, and that about 94% of 4π sr·yr lies within the field of view of three or more facilities.

Existing multimessenger searches involving only pairs of observatories are typically in a master–slave relationship, e.g., a triggering observatory initiates follow-up at an optical telescope [78–80]. In contrast, AMON will enable archival and real-time searches for coincidences among multiple observatories in a peer-to-peer relationship that will provide markedly increased opportunity for discovery of new multimessenger sources, as detailed in Section 4 below. The real-time AMON analysis will be informed by the extensive effort already invested by the triggering observatories [78,81–90]. The trigger events these observatories produce will

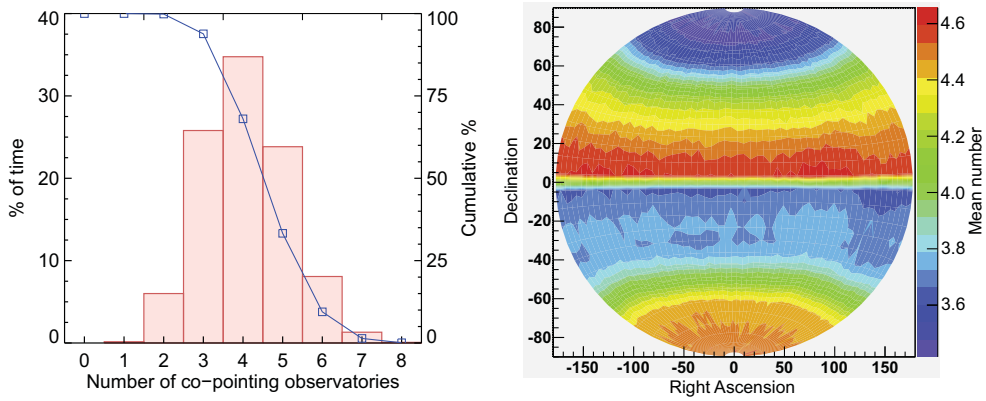

Fig. 1. (left) Distribution of the total number of trigger facilities observing a cosmological source, averaged over time and sky location. (right) Average number of observatories simultaneously viewing a source, as a function of location. Spatial variance is caused by the limited field-of-view of some observatories and the movement of orbital telescopes.

be heterogeneous, covering the full range of messenger particles and differing significantly in background rate and localization precision. In some cases the events will include additional quality information that may be useful in refining the single-stream false positive rate. For purposes of AMON, all events will be couched in the common language of statistics, containing information including a trigger time, event position, and a positional error or probability density function (PDF).

Once the individual event streams have been characterized, including tracking observatory pointing and FPR, the multiple event streams can be combined. At the most basic level, this will be carried out via a coarse clustering analysis, searching for temporal and spatial coincidences. The output of the clustering analysis is dominated by pairwise coincidences, with the FPR for an ordered pair of triggers from observatories (a, b) given by,[2]

$$R_{ab}^{(\mathrm{FP})} \approx \frac{R_a}{\Omega_a}\frac{R_b}{\Omega_b}\Delta T\langle\Omega_{ab}\rangle\Delta\Omega_{ab}, \tag{1}$$

where R_a is the subthreshold event rate from observatory a to AMON (assumed constant here), Ω_a is the field of view of observatory a, ΔT is the total width of the temporal search window, $\langle\Omega_{ab}\rangle$ is the time-averaged overlapping field of view of observatories a and b, and $\Delta\Omega_{ab}$ is the search area for coincidences between observatories a and b. In Table 1 (row "b"), we show the result of this calculation for $\Delta T = 100$ s and $\Delta\Omega_{ab}$ adjusted to give ~90% acceptance for signal event pairs (where each event is at the threshold for transmission to AMON). The self-coincidence of the individual observatories is given by the diagonal R_{aa} (although this calculation is not appropriate in the case of preprocessed event streams) and the sum $R_{ab} + R_{ba} (a \neq b)$ gives the total number of pairs from a and b without respect to order. As expected, the combined FPR due to a pair of false positive events is orders of magnitude lower than that of the individual component subthreshold event streams.

This particular calculation is by no means definitive. A trivial adjustment of the cuts will increase the rates (useful for generating AMON Alerts for testing purposes). More importantly, additional information can drastically lower the FPR for the AMON analysis (Table 1, row "c"). For example, one can statistically stack the Alerts though an archival study, or shorten the temporal search window to search for exotic phenomena. In real-time, one can require that at least one event be of high significance or that the coincidence contains at least three events.[3]

A promising feature of AMON is its ability to distribute Alerts in real-time to initiate follow-up observations. The relatively high FPR represented by the sum total of all pairwise coincidences among the observatories considered (Table 1, row "b") may be tolerable for some follow-up facilities, especially if their response is highly automated. However, many follow-up facilities will have limited observing time available for this science and may require a substantially lower FPR for triggering. This can be achieved via a refined analysis, providing a combined best fit location and error, as well as a maximum likelihood ratio or Bayesian probability. The likelihood or probability measure is drawn from a continuous distribution, in contrast to the FPR of the clustering analysis which, given a fixed event rate for each stream and a fixed set of cuts, takes on a unique value for any pair of event streams. Prior information can easily be incorporated into the likelihood analysis including, for example, previous detection limits, observatory sensitivity, or a galaxy catalog, and these choices can be tuned for different follow-up programs.

As an independent channel of scientifically-relevant data and constraints, follow-up observations have the potential to provide the added information required for a definitive discovery. By distributing candidate source positions in real-time to follow-up facilities, with statistically valid measures of the FPRs, AMON will enable efficient fast-response counterpart searches and studies across the electromagnetic spectrum. The existence and nature of such EM counterparts may prove decisive in verifying the existence of some of the first multimessenger sources, and can reveal the nature and detailed properties of the source, including important ancillary information such as the source environment, host galaxy (if any), and properties of intervening gas and dust along the line of sight. The discovery potential of pairwise coincident events with positive follow-up detection is described in more detail below.

AMON will be deployed in three phases. During the first year of

[2] In some cases, it may be advantageous to use one event stream to trigger event selection for another, e.g., if the rate of single events is high, as with HAWC, or if the localization is poor, as with low-significance gravitational wave events. However, processing of an observatory's data can always be carried out, either at AMON or prior to transmission, to yield a manageable single-observatory FPR, and such preprocessing has been assumed for this discussion.

[3] The FPR for a coincidence of the ordered triple (a, b, c) is given by $R_{abc}^{(\mathrm{FP})} \approx \frac{1}{2}\frac{R_a}{\Omega_a}\frac{R_b}{\Omega_b}\frac{R_c}{\Omega_c}(\Delta T\Delta\Omega_{abc})^2\langle\Omega_{abc}\rangle$, where the factors $\Delta\Omega_{abc}$, an equivalent search area for a threefold coincidence, and $\langle\Omega_{abc}\rangle$, the joint field of view, are determined by Monte Carlo. The factor of $\frac{1}{2}$ depends on how the temporal search is defined, where here we require that all three events occur within ΔT. In Table 1c, we present the totals $\sum_{bc} R_{abc}^{(\mathrm{FP})}$, for the case where all Auger data is included and for the case where Auger data is restricted to the galactic plane.

operation beginning in mid-2013, AMON will use archived data to develop and tune analysis algorithms. Such archival analyses, while a necessary first step prior to activation of real-time alerts, will also be of intrinsic scientific interest, and may point to possible new astrophysical signals or new and constraining upper limits on jointly-emitting source populations. Even as AMON moves toward real-time operation, certain source populations will be best discovered through a collaborative blind study of accumulated data; for example, in searches for exotic particles, as discussed below for primordial black holes. To enable this, participating AMON members will, at any time, be able to utilize the AMON database and data products, under rules that are established in the AMON MOU [91].

In subsequent operational phases, standard AMON analyses will be modified to operate in real-time, enabling identification of candidate transient sources as soon as the events are transmitted. At first, the effort will focus on those discoveries that can be made by the triggering facilities alone, with FPRs similar to those in Table 1c. Even at this stage, the real-time nature of the network plays a critical role, providing the triggering facilities with AMON Alerts that can prompt a closer analysis of their own data. The Alerts shared at this stage will include many whose combined FPR is too high to claim detection of a transient. These will not only exercise the AMON system, but may initiate a deeper search by those participating observatories that did not initially report a triggering event. An example of this discovery mode is the joint search for high-energy cosmic neutrinos and gravitational waves, as discussed below.

As quickly as is feasible, AMON will transition to its final phase, with Alerts distributed to participating follow-up observatories to enable the near real-time search for electromagnetic counterparts. For sources that exhibit detectable afterglow, this is the most powerful technique, leveraging the high acceptance of the initial FPR threshold, yet resulting in a final FPR that is lower than that available by the other techniques. The estimated final FPRs are shown in Table 1c, for the case of serendipitous follow-up detection of GRB afterglow (assuming Swift XRT sensitivity and a $\sim 1^\circ$ search region) or a SNe light curve (assuming the detection limits of [78]). In the next section, as a proof of concept, we show that significant sensitivity gains are made by AMON in the search for electromagnetic counterparts to cosmic neutrino sources.

4. Discovery power of AMON

In this section we attempt to quantify the discovery power of AMON. Any such effort must grapple in some way with the vast array of possible discoveries that AMON might contribute to, both in terms of the various candidate source populations (Section 2) and in terms of the diverse set of possible partner facilities (Section 3), including the combinatorial implications of joining those facilities together into a single network.

We take two distinct approaches here. In the first approach, we focus on three specific examples of multimessenger source populations, construct models for the populations and their multimessenger signals, and simulate the performance of appropriate partner facilities both with and without the contributing capabilities of AMON. Specifically, Section 4.1 examines how the distribution of AMON Alerts can greatly enhance the search for electromagnetic counterparts to candidate sources of cosmic neutrinos, while Section 4.2 quantifies the gains for a search for joint sources of gravitational waves and CN. Section 4.3 discusses an example search for exotic phenomena, showing how an AMON analysis may provide the first clear signature for primordial black holes.

In the second approach, we explore the sensitivity of the various possible AMON partner facilities in a relatively model-independent fashion (Section 4.4). The diverse array of messenger types, above-threshold and sub-threshold trigger definitions, and likely source populations (e.g., Galactic, Local Group, Extragalactic, cosmological) addressed simultaneously in this analysis make an assumption-free exploration impossible; however, we have adopted a relatively simple set of default assumptions that at least enable the cross-facility comparison to be made. In doing so, we address the merits and demerits of this approach as compared to our preferred simulations-based method.

4.1. Follow-up of candidate cosmic neutrino sources

As a first example, we consider the follow-up imaging of candidate cosmic neutrino sources. Such searches are already underway via efforts by individual neutrino observatories and their follow-up partners. For example, in [92], the IceCube Observatory identifies clusters of two or more neutrino events as a trigger for follow-up imaging. Due to the high rate of atmospheric neutrinos and other backgrounds, the expected FPR for a pair of up-going events for IceCube-86 is approximately 30 yr^{-1} (Table 1, row "b"). Alerts are then distributed to the ROTSE telescope array or, after using a maximum likelihood analysis to refine their number, to Swift and PTF [80,93]. This program is already producing the first limits on SNe with choked jets [78].

As a shorthand, we introduce the notation "2ν" to indicate a trigger condition of 2 or more coincident neutrinos, or ν-$N\gamma$ for one or more neutrinos and N or more γ-rays. To be concrete, we study the follow-up imaging of 2ν alerts at a rate of 10 yr^{-1} using Swift's co-aligned X-ray and UV/Optical Telescopes (XRT, UVOT), with this considered a *status quo* approach for the scientific community. Due to the narrow field of view (0.4° diameter) of the XRT and UVOT, 7 Swift pointings are required to cover the error region of each alert, totaling 70 pointings in all.

In contrast, the AMON approach enables the realtime coincident analysis of neutrino and electromagnetic data streams, comparing the arrival time and direction of a *single* candidate CN with data from Swift's large field of view Burst Alert Telescope (BAT), Fermi's Large Area Telescope (LAT), or the upcoming ground-based HAWC. Because of the superior AMON localizations, derived via the joint analysis with high-energy γ-rays, the same follow-up telescope resource (70 pointings) can be used for follow-up of a significantly-increased number of AMON alerts. Here we consider a program that follows up five 2ν alerts (at 7 pointings each) and 35 ν-$N\gamma$ alerts (1 pointing each). For the ν-$N\gamma$ alerts, we considered the pairing of IceCube with both BAT and LAT.

The relative sensitivity of the *status quo* and AMON approaches was studied via a Monte Carlo calculation. As a source model, we assumed that both γ-ray and neutrino spectra follow a broken power-law with initial and final logarithmic slopes of $\alpha = 1.0$ and $\beta = 2.0$, and break energies $\mathscr{E}_\gamma = 0.2$ MeV and $\mathscr{E}_\nu = 0.35$ PeV, respectively. The neutrino and γ-ray fluence was allowed to vary, as indicated by the axes of Fig. 2. Using realistic models for the IceCube-86, BAT, and LAT effective areas, point spread functions, and their overlapping field of views, we were able to determine the acceptance of each simulated source. Realistic background models were adopted for each observatory, enabling the calculation of false positive rates for each joint analysis.

In each case, the FPR was tuned via a likelihood analysis of the relative position of the ν and γ events. Subthreshold BAT and LAT events were allowed into the simulated data stream, with terms added to the likelihood function to favor the more significant EM signals. Furthermore, we added a regulating term to the likelihood function to account for the possibility of a real γ-ray source in accidental coincidence with an IceCube background event (e.g., an atmospheric neutrino). Once the FPR is chosen for any pair of observatories, we identify the required likelihood threshold, and can then calculate the corresponding sensitivity to our modeled

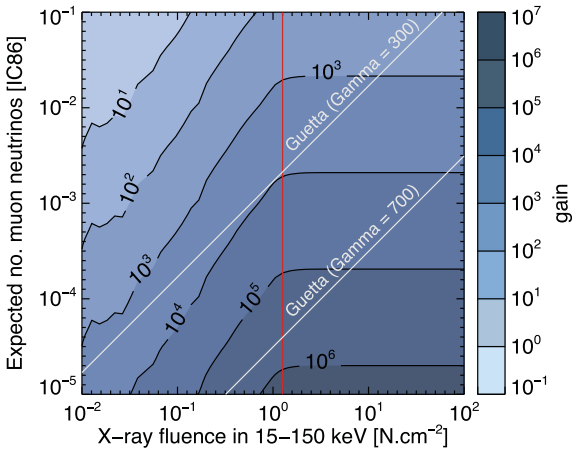

Fig. 2. Sensitivity of the AMON multi-channel method compared to the *status quo*, presented as a ratio ranging up to $\sim 10^6$, for follow-up observations of candidate astrophysical neutrino sources. The assumed shapes for both gamma and neutrino spectra follow a broken power law with initial and final logarithmic slopes of $\alpha = 1.0$ and $\beta = 2.0$, and break energies $\mathscr{E}_\gamma = 0.2$ MeV and $\mathscr{E}_\nu = 0.35$ PeV. The vertical line shows a typical threshold for a hard X-ray observatory (e.g., Swift BAT), and diagonal lines corresponding to predicted neutrino to gamma-ray fluxes under a range of current theoretical GRB models [22].

source. While the initial FPR is quite high (10–70 alerts yr^{-1}), the final FPR will be orders of magnitude lower after the inclusion of follow-up data and, as such, can be ignored in the study of sensitivity. While here we have characterized the sensitivity of the triggering methods (AMON versus *status quo*), there are a number of unknown factors in the sensitivity of the subsequent follow-up searches; for example, due to optical magnitude. However, we study the ratio of the sensitivity of the two methods, expecting the acceptance of the two follow-up programs will be approximately the same and to cancel in the ratio.

The results are shown in Fig. 2, where substantial gains in sensitivity (up to 10^6) are realized. The sensitivity of each method is defined as the fraction of true sources pursued using a given follow-up capability. In addition to enabling pursuit of an increased number of alerts overall, the AMON approach realizes these large sensitivity gains by triggering from *single* neutrinos rather than a neutrino pair, leveraging the increased interaction strength of γ's over ν's. The left axis of Fig. 2 is defined in such a way that it could equally well describe the expected event rate for ANTARES, with only a small change in the contours due to the narrower neutrino point spread function.

Gains of this type have also been demonstrated for gravitational wave source searches, using GW-γ triggering over the *status quo* GW-only methods [94]. For GW-only searches, the poor GW localization is filtered by requiring coincidence between the GW localization and a nearby cataloged galaxy [79,95]. While useful, this approach suffers from several shortcomings: First, it depends on the completeness and astrophysical relevance of the associated galaxy catalog; second, it cannot be extended to the subthreshold regime due to the dramatic increase in false alarm rates; and finally, the approach is limited to an horizon of $\lesssim$100 Mpc, beyond which galaxy fields become crowded and catalogs are highly incomplete. The multi-channel, multimessenger approach by contrast provides a unique candidate source position for follow-up pointing, and leverages the coincidence technique to push into the subthreshold, possibly revealing otherwise-undetectable source populations. With Advanced LIGO expected to ultimately achieve sensitivity out to $\gtrsim$ 500 Mpc [96], the AMON approach can offer a >125-fold gain in sensitivity for events with bright EM counterparts, or >1000-fold for regions that have the least complete galaxy catalog.

Table 2
Effective volumes for a joint GW-CN search, assuming $E^{\rm iso}_{\rm GW} = 10^{-2} M_\odot$ and $E^{\rm iso}_\nu = 10^{49}$ erg for a choked GRB model.

Analysis	Integration limit (Mpc)	Neutrino threshold	$V^{(\rm eff)}$ [Mpc^3]
GW+CN	80	$n_\nu \geqslant 3$	4.6×10^2
AMON	160	$n_\nu \geqslant 1$	5.9×10^4

4.2. Joint detection of neutrinos and gravitational waves

Here we consider the joint detection of gravitational waves and high energy cosmic neutrinos as an example of a science investigation enabled by the realtime operation of AMON. The search for jointly emitting GW+CN sources has been addressed in [97,98], including predictions for Advanced LIGO-Virgo and IceCube-86, and we follow the same general approach (see also [99,100]). However, while previous authors focus on the joint analysis of a multi-messenger data archive, we emphasize the possibility of carrying out this analysis in realtime. We characterize the sensitivity of a blind (untriggered) search by Advanced LIGO-Virgo using the horizon distance $D_{\rm GW}$, inside which a GW source is expect to generate an above-threshold detection,

$$D_{\rm GW} \approx 80\ {\rm Mpc} \left(\frac{E^{\rm iso}_{\rm GW}}{10^{-2} M_\odot} \right)^{\frac{1}{2}}, \tag{2}$$

where $E^{\rm iso}_{\rm GW}$ is the isotropic equivalent gravitational wave energy of the source. This is based on the results of [101] and assumes little of the GW waveforms. Without AMON-like infrastructure, a realtime detection of both GW and CN requires that a source be within this horizon and that it produce a neutrino flux sufficient to trigger $n_\nu \geqslant 3$ events in IceCube or ANTARES (since $n_\nu \leqslant 2$ would lead to an inconclusive false positive rate). These detections would then be compared *post facto*, either through an archival analysis or *above-threshold* alert distribution (e.g., through GCN), to determine if there are any joint GW-CN sources.[4]

By contrast, a system like AMON will provide two-way communication between observatories, enabling a realtime triggered search of GW data, either by transmission of pre-alerts from AMON to LIGO-Virgo or by carrying out a triggered search on subthreshold GW data transmitted to AMON (albeit in some preprocessed form). Searches of this kind suffer a lower trials penalty and may assume various templates for the sources. For example, the postulate that CN are detected in coincidence allows one to make an assumption about the orientation of the source, making the GW signal more favorable for detection [102]. In all, we estimate that these effects will combine to increase the horizon distance to $2 \times D_{\rm GW}$ [102]. Furthermore, only a single neutrino event is required to trigger the analysis, providing significant gain for this approach since the expected number of neutrinos has been observed to be typically $\ll 1$ [103].

Since we are considering the relatively deep horizon distance for Advance LIGO-Virgo (so that galaxy distribution can be assumed uniform), but not so far that redshift effects become important, it is sensible to apply the effective volume approach of A, integrating up to the physical limit of $D_{\rm GW}$ or $2D_{\rm GW}$. The resulting effective volumes are given in Table 2.

Under the assumption of a low false positive rate, the 90% upper limit (chosen for consistency with [97]) for the joint GW-CN source density is given by

[4] In [97], the authors consider a slightly different problem, being interested in the above-threshold detection of GW or CN. While an interesting measure, their calculations do not provide the sensitivity for above-threshold detection of joint sources that we need for comparison to AMON.

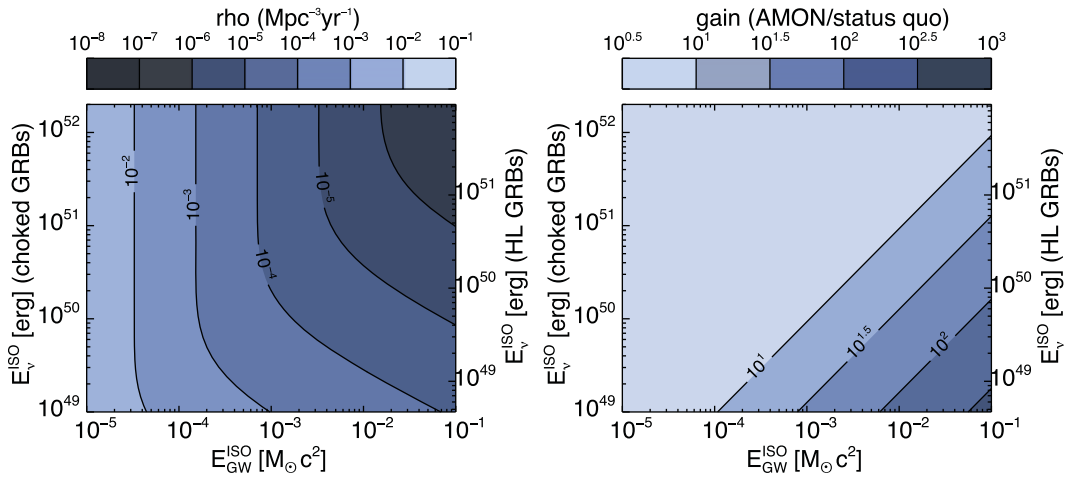

Fig. 3. (Left) Projected GW+CN source population upper limits after one-year of AMON utilizing observations with Advanced LIGO-Virgo and IceCube-86. (Right) Ratio of the sensitivity for the AMON approach to the sensitivity of the *status quo*approach (as described in the text).

$$\rho_{\text{GW-CN}} < \frac{2.3 f_b}{T V^{(\text{eff})}} \quad [\text{yr}^{-1}\ \text{Mpc}^{-3}], \tag{3}$$

where T is the livetime, which we take to be one year, $V^{(\text{eff})}$ is the solid angle averaged effective volume for the given method, and f_b is the beaming factor for neutrinos. We take the latter to be $f_b = 14$ (from [97]) but it will cancel in our final result.

The effective volume depends on $E_{\text{GW}}^{\text{iso}}$ through Eq. 2. For neutrinos, the expected number of detections from a fiducial source at distance r can be related to the neutrino isotropic energy E_ν^{iso}, using a linear relationship provided in [97],

$$n_\nu \approx \frac{1}{\kappa}\left(\frac{E_\nu^{\text{iso}}}{10^{49}\ \text{erg}}\right)\left(\frac{10\ \text{Mpc}}{r}\right)^2, \tag{4}$$

where, for IceCube-86, $\kappa = 0.75$ for a high luminosity GRB model and $\kappa = 1.6$ for a model of choked GRBs.

The results are shown in Fig. 3. The left side shows the upper limit in units of yr^{-1} Mpc^{-3} that would be obtained by a non-detection with AMON. The right side shows the multiplicative gain in sensitivity that the AMON approach provides over an analysis that requires above-threshold detection in both GW and CN channels. The gain is most significant for bright GW sources and weak neutrino sources, where the burden for discovery is shifted from the CN to GW channel. However, the gain is strictly greater than 1, with an asymptote of 8, representing the increase in effective volume due to triggering the GW search.

4.3. Searching for primordial black holes

Here we consider the search for primordial black holes as an example of a collaborative study of accumulated multi-facility data, as enabled by the AMON infrastructure and data sharing policies. In particular, we have modeled a joint search with the IceCube neutrino observatory, HAWC TeV gamma-ray observatory, and the Pierre Auger cosmic ray observatory. All are sensitive to particles produced in the final stages of PBH evaporation, including a potential signal from ultrahigh-energy neutrons detected at Pierre Auger, since these neutrons would not suffer from the magnetic deflection and time delay effects of charged cosmic rays (the chief UHE neutron background).

Based on the energy threshold of these experiments and energy dependence of various models predicting energy spectra of PBHs in their final stage of evaporations (e.g. [104–106]), the model of a non-rotating, uncharged black hole without a chromosphere by MacGibbon and Webber [104] was chosen for estimation of the expected signal at each of these detectors. The time integrated particle spectra above 100 GeV were computed following methods from Refs. [107,104,108,109]. The main particle decay chains considered in our calculations are described in B.

It is anticipated that, when fully operational, HAWC by itself will either detect or provide the best upper limit on direct searches for PBH decay, around 2 orders of magnitude better than the current upper limit (as shown in Fig. 4). To do so, HAWC must perform a blind search of its own data. After a cut to remove many hadronic events, 5.1 kHz of subthreshold trigger events remain, which will be analyzed for coincidences across a spatial template with 10^4 trials [110]. Taking a generous time window of $\Delta T = 5$ s and a number threshold of $n \geqslant 20$, the HAWC false coincidence rate can be reduced to <1 yr^{-1}. However, it is expected that HAWC will also observe real astrophysical transients that are unrelated to PBHs, forming a second type of false positive for the PBH search. We conservatively estimate this number to be $R_1^{(\text{FP})} < 17$ bursts per year, approximately equal to the known LAT GRB rate, allowed to fluctuate up by 2σ. If, after $T = 1$ yr of livetime, 17 unidentified bursts were observed, the 99.73% (3σ) upper limit for PBH would be given by

$$\rho_{\text{PBH}} < \frac{32.1}{V^{(\text{eff})}} \quad \left[\text{yr}^{-1}\ \text{pc}^{-3}\right], \tag{5}$$

where 32.1 is chosen to give the 99.73% upper limit of the Poisson distribution, and $V^{(\text{eff})}$ is the integral of the trigger condition $P(n \geqslant 20|r)$ over $4\pi r^2 dr$, averaged over solid angle, where r is the distance from the Earth. The value of $V^{(\text{eff})}$ is specific to the sensitivity of the observatory and the intrinsic γ-ray fluence of the fiducial source, and is further described in A. For the current calculation, we estimate $V^{(\text{eff})} = 0.037\ \text{pc}^{-3}$. The calculated value of $\rho_{\text{PBH}} < 3.5 \times 10^3\ \text{yr}^{-1}\ \text{pc}^{-3}$ can be compared to the current best limit of $1.9 \times 10^5\ \text{yr}^{-1}\ \text{pc}^{-3}$ from VERITAS [111].

Between the current VERITAS limit and the projected HAWC limit, there exists the possibility of a future positive detection of PBH decays. However, the HAWC data by itself may be unable to distinguish between PBH and other scenarios. A joint AMON study of HAWC data with neutrino and neutron data (modeled here with IceCube and Auger), will enable the search for multimessenger coincidences, providing a unique PBH signature. Just a few such coincidences should reveal a timing and energy structure that are indicative of Hawking evaporation.

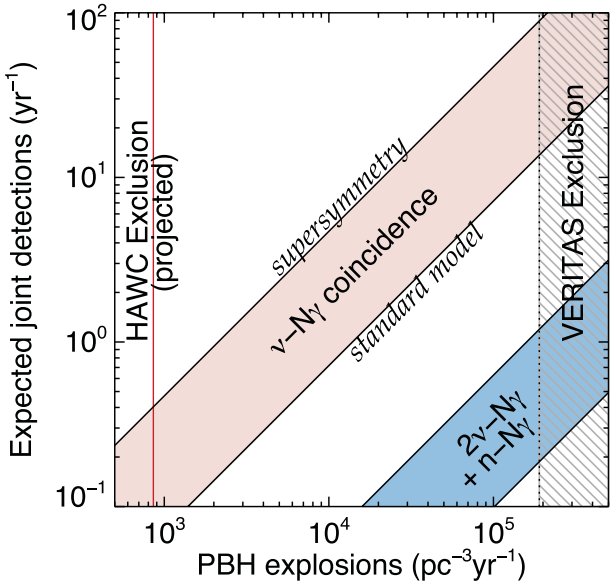

Fig. 4. Expected number of sources detected in at least two of the ν, γ, and n channels, modeled here with the IceCube-86, projected HAWC, and Auger sensitivity, as a function of the primordial black hole density. The shaded region to the right indicates PBH densities that previous direct searches have excluded, while the vertical line shows where the upper limit is expected to move if HAWC does not observe a gamma ray excess after a year of livetime. In between, there is the possibility of positive joint detections, with potentially a unique PBH signature.

Table 3
Effective volumes for multimessenger PBH search. Values are averaged over 4π sr, with only those regions of overlapping sensitivity contributing to each pairwise calculation.

Observatories		Trigger conditions		$V_{SM}^{(\mathrm{eff})}$ [pc^3]	$V_{SUSY}^{(\mathrm{eff})}$ [pc^3]
A	B	A	B		
HAWC	–	$n_\gamma \geqslant 20$	–	0.0374	0.245
IceCube	HAWC	$n_\nu \geqslant 1$	$n_\gamma \geqslant 13$	9.8×10^{-5}	6.4×10^{-4}
IceCube	HAWC	$n_\nu \geqslant 2$	$n_\gamma \geqslant 13$	1.3×10^{-6}	8.3×10^{-6}
HAWC	Auger	$n_\gamma \geqslant 13$	$n_n \geqslant 1$	1.3×10^{-7}	8.6×10^{-7}
Auger	IceCube	$n_n \geqslant 1$	$n_\nu \geqslant 1$	4.9×10^{-9}	3.2×10^{-8}

Folding together the PBH source model from B and the volume integrals of A, we calculate the effective volumes given in Table 3. To maximize sensitivity to neutrinos and neutrons, we use number thresholds of $n_\nu \geqslant 1$ and $n_n \geqslant 1$. For γ-rays, the low false alarm rate can be relaxed significantly by requiring coincidence with a single ν or n, allowing the HAWC threshold to be lowered to $n_\gamma \geqslant 13$. The expected rate of *true positive* joint detections in channels a and b is then given by

$$R_{ab}^{(\mathrm{TP})} = \frac{\rho_{\mathrm{PBH}}}{V_{ab}^{(\mathrm{eff})}} \quad [\mathrm{yr}^{-1}\ \mathrm{pc}^{-3}], \tag{6}$$

which we show as a function of ρ_{PBH} in Fig. 4. Over the range of ρ which might lead to future positive detections by HAWC, the total number of expected multimessenger coincidences ranges from 0.1 to 100 yr^{-1}. Most of these are ν-$N\gamma$ (i.e. a coincidence between a single neutrino and N γ-rays). However, there is a non-negligible possibility for observing n-$N\gamma$ coincidences (where the neutron is detected by Auger) or 2ν-$N\gamma$, providing an exciting possibility for detecting three subthreshold events in coincidence (where the $N\gamma$ from HAWC are treated as a single subthreshold event).

4.4. Cross-facility sensitivity comparison

In general, our preferred approach to evaluating the discovery power of AMON has been via direct simulation of modeled source populations as in the sections above. The chief shortcoming of this approach is that, by focusing on individual case studies, it fails to provide a comprehensive overview of the discovery space that will be opened up by the array of multimessenger facilities now coming online – and by AMON itself.

For completeness, then, in this section we present a relatively model-independent cross-facility comparison of the sensitivity of candidate AMON partner facilities.

Before presenting this analysis, however, we wish to point out some key limitations. First, quantifying the discovery power of a multimessenger search is intrinsically and strongly model-dependent. For example, the relative probability of triggering a high-energy γ-ray observatory compared to a low-energy X-ray observatory depends strongly on the spectral shape of the source, with a steeply-falling spectrum favoring the low-energy facility, and relatively hard spectra favoring the high-energy facility.

Second, the discovery power of AMON depends critically on the joint multimessenger emissions of entire populations of sources. For example, jointly emitting $\nu\gamma$ sources (e.g., HL-GRBs) may be routinely detected in gamma-rays and undetected in neutrinos. However, given a large population of such sources (e.g., hundreds of HL-GRBs per year with current satellites), each with low neutrino fluences, occasionally one source will yield detection of a single neutrino. Modeling the source population as in Section 4.1 allows us to take this "rare but significant" scenario into account when calculating the increased discovery power of AMON for jointly-emitting $\nu\gamma$ sources.

Finally, the ability to make joint detections via two or more messenger types depends critically on the relative energy fluences in each channel. Yet the fluences in different channels are not generally expected to be equal, and in some cases are not even expected to be well-correlated (except for the correlation induced by observing sources across a substantial range in distance). In general such effects can only be addressed realistically via source-specific simulations. For example, the total energy emitted in very high energy (VHE) neutrinos and γ-rays by HL-GRBs (and potentially LL-GRBs) is expected to be comparable in some models; however, the VHE γ-ray emissions will be strongly attenuated by interactions with the extragalactic background light beyond a relatively short cosmic horizon of $D \sim 1$ Gpc.

For purposes of our cross-facility comparison, we ignore these effects and choose a single standard source spectrum, a power-law with spectral slope $dN/dE \propto E^{-2}$. This is the same spectrum as used in Section 4.1, but different from the spectra used in our other examples. The spectrum is extrapolated without any break to lower energies when needed, which also differs from our approach in the source specific examples. The chief advantage is that it enables comparison of observatories operating at radically different energies using the single parameter F_γ, defined via

$$\frac{dN_\gamma}{dEdA} = \frac{F_\gamma E^{-2}}{\ln 10}. \tag{7}$$

Defined in this way, F_γ is the gamma energy fluence (eV cm^{-2}) *per decade* of energy.

For neutrinos and neutrons, we use the same E^{-2} shape and replace the normalization parameter F_γ with F_ν or F_n, as appropriate, for the neutrino or neutron energy fluence per decade. We note again that EeV neutrons will only be detectable for sources within the Galaxy. The various parameters F_γ, F_ν, and F_n can then be represented on a single axis in the same figure. However, naturally these remain entirely different quantities, representing the energy

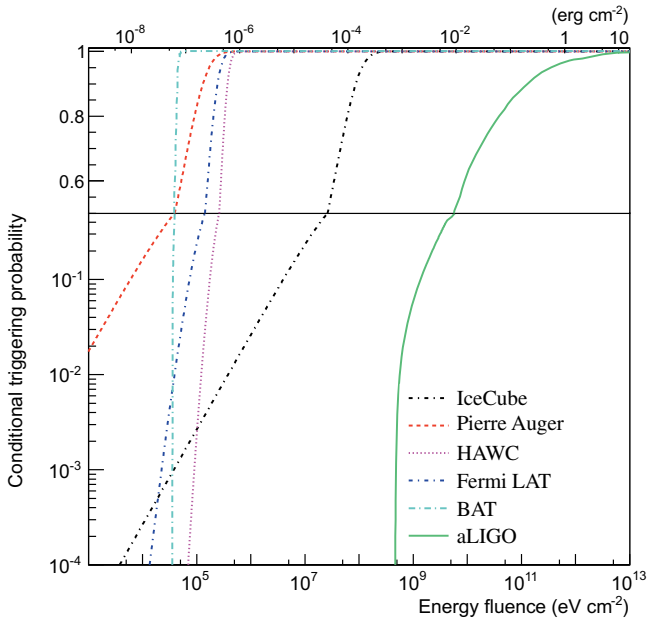

Fig. 5. Conditional triggering probability P as a function of energy fluence F (with linear scale for $P \geqslant 0.5$ and log scale for $P < 0.5$), assuming the source is in the field of view and the observatory is active. For BAT, LAT, HAWC, IceCube, and Auger, the bottom axis shows the fluence per decade under the assumption of an E^{-2} spectrum while, for the Advanced LIGO model, total fluence is shown.

fluence per decade at Earth for the associated messenger only, without any implication that likely source models are expected to emit the different messenger particles in equal or fixed proportion. Completing a characterization of cross-facility sensitivities would require adjusting for the emission properties of a specific source population, as in our simulations, and accounting for any propagation effects that would affect the fluences observed at Earth.

Finally, we can incorporate gravitational wave detection into the same scheme by following the equations of Section 4.2 and using the shape of the efficiency curves from [101]. We assume that a total GW energy of $0.01 M_{\odot} c^2$ will produce a GW event at the nominal detection threshold when located at 160 Mpc from Earth (assuming coincidence with some other messenger type in AMON). We note that the total event fluence F_{GW} derived in this way is fundamentally different from the F_{γ}, F_{ν}, and F_n fluences, which are defined as fluences *per decade*. At the same time, we note a strong expectation that, for the strongest GW transients, the GW energy release will be orders of magnitude greater than for any other messenger type.

The result of these calculations is presented in Fig. 5 as a plot of the conditional trigger probability P for each AMON partner facility versus the event fluence or fluence per decade for the appropriate associated messenger, as defined above. The conditional trigger probability is the probability of detection for an event occurring within the facility field of view while the facility is in active operations at nominal expected sensitivity.

In order to derive a single conditional probability of triggering for any event of particular fluence, we have made some further assumptions. With respect to the γ-ray facilities BAT, LAT, and HAWC, we assume that the energy fluence arrives in one second and that the observatory is set to trigger on one-second bursts; as a trigger threshold, we require that the expected number of event photons exceed the expected background in this interval over a region sized to the facility PSF. This approach leads to a steeply-rising trigger probability as the threshold condition is approached and exceeded. Moreover, we note that the ordering of sensitivities shown in the plot for BAT, LAT and HAWC depends strongly on the spectral model. Had we chosen to break the spectrum, making it flatter at low-energy, then LAT and HAWC would have been more competitive relative to BAT.

For each observatory, we can identify a nominal threshold corresponding to $P = 50\%$ conditional triggering probability, which we see occurs at $F_{\gamma} \lesssim 10^5$ eV cm^{-2} for BAT, LAT, HAWC. In contrast, IceCube has a greater nominal threshold of $F_{\nu} \sim 10^8$ eV cm^{-2}. Among events with comparable γ-ray and neutrino fluences (at Earth), only the very brightest γ-ray sources would be expected to yield enough neutrinos to exceed this threshold. However, as discussed above, an occasional neutrino detection can also be anticipated as the result of statistical fluctuations among a much larger population of weaker sources. By virtue of AMON coincidence analysis, this neutrino detection can be assumed to be effectively background-free, which results in a sensitivity curve that rises much less steeply than that of the γ-ray observatories. Specifically, at $F_{\nu} = 10^5$ eV cm^{-2}, two or three of 10^3 sources would be detectable in neutrinos, a possibility that is highly relevant both for GRBs and for possible unknown source populations.

With respect to the Pierre Auger Cosmic Ray Observatory, Fig. 5 apparently shows a "best of both worlds" situation, with a relatively low nominal threshold of $F_n < 10^5$ eV cm^{-2} and a gently falling trigger probability below that. This has the same shape as IceCube's $P(F)$ curve, given by the Poisson probability of contributing at least one event to a coincidence analysis, but with a higher event yield for a given fluence. However, it should be recalled that the Auger calculation is for neutron events only, which probe a highly limited detection volume due to their half-life. Furthermore, the assumed E^{-2} spectrum cannot extend indefinitely to high energy lest it require infinite energy at the source; steeper spectra, or spectra with breaks within or below the Auger range, would reduce the relative sensitivity of Auger by comparison to the other facilities.

We conclude that, while a unified presentation of cross-facility sensitivities can be achieved (Fig. 5), the results retain a significant number of assumptions such that interpreting the figure, and translating it into real-world expectations for actual cosmic events, is not straightforward.

5. Summary and conclusions

The Astrophysical Multimessenger Observatory Network under development at Penn State will link multiple high-energy, multimessenger, and follow-up observatories together into a single comprehensive system. We have explored the scientific opportunity for AMON (Section 2), which is centered on the discovery and exploitation of multimessenger transients. The nature of the brightest such transients, which may manifest as the first detections of gravitational waves, high-energy cosmic neutrinos, or high-energy cosmic ray neutrons, is still unknown; likely candidates include blazar flares and a diverse array of $\gamma - ray$ bursts and supernovae, as well as exotic phenomena such as the evaporation of primordial black holes from the early universe.

We have described the design, infrastructure, and current and projected partner facilities of AMON (Section 3), showing that the wide fields of view, high duty cycles, and subthreshold event rates of the facilities are such that a robust and automated statistical search for coincident events seen in the data of two or more facilities is both interesting and feasible (Table 1). In particular, false positive rates for the resulting AMON Alerts are sufficiently low that comprehensive ground-based optical follow-up campaigns can be contemplated.

With neutrino and γ-ray observatories are already participating in AMON, and discussions underway with cosmic ray and

gravitational wave observatories, as well as multiple follow-up observatories, AMON is poised to begin real-time operations within a year.

To demonstrate the power of the AMON approach, we have carried out three sets of simulations using current theoretical models of multimessenger phenomena, and compared the sensitivities of the various multimessenger facilities to one another using a somewhat simplistic ansatz (§4). In the first simulation, we explored the challenge of EM counterpart searches for candidate GRB-associated CN observed in IceCube, showing that vetting candidate CN events against multiple EM data streams realizes a >1000-fold gain in the efficiency of EM follow-up observations (Fig. 2). In the second simulation, we explored the improvement in search sensitivity for jointly emitting GW+CN transients that is realized by extending these searches into the subthreshold regime, rather than restricting the search to events that generate statistically-significant signals in both channels; we find that a >10-fold increase in event rates, or improvement in upper limits, is easily achieved (Fig. 3). In the third simulation, we explored the multimessenger signature of PBH evaporation, demonstrating that – consistent with current upper limits on the local PBH density – the coincidence of an IceCube-detected neutrino with a cluster of HAWC-detected γ-rays could provide evidence for observation of a PBH evaporation event within the first year of HAWC operations (Fig. 4). The promise and challenges of multimessenger transient detection seen in these three case studies are also illustrated, in wider reaching but less readily interpreted fashion, by our cross-facility sensitivity comparison (Fig. 5).

In addition to carrying out the real-time multi-facility transient searches needed to realize these and other science gains, and enabling follow-up EM observations by distributing transient alerts to interested observers, AMON will provide a framework for large observatory collaborations to work together on targeted archival analyses using AMON's comprehensive events database and coincidence analysis toolkit. In these several ways, AMON will leverage and enhance the capabilities of existing and future high-energy and multimessenger observatories, powering a new and ambitious exploration of the transient universe using all four forces, and so helping to realize the immense promise of this dawning age of multimessenger astronomy.

Acknowledgements

Initial development of AMON has been funded by Penn State's Office of the Senior Vice President for Research, the Eberly College of Science, and the Penn State Institute for Gravitation and the Cosmos. D. F. Cowen acknowledges the support of the Penn State Institute for CyberScience Faculty Fellows Program; I. Bartos and S. Márka acknowledge support from Columbia University and the National Science Foundation under cooperative agreement PHY-0847182.

The authors acknowledge valuable discussions and inputs from Jürgen Brunner, James Chiang, Alessandra Corsi, Farhan Feroz, Sam Finn, Anna Franckowiak, Gabriela Gonzalez, Jordan Goodman, Kazumi Kashiyama, Jim Matthews, Julie McEnery, David Miller, Prasenjit Mitra, Tom Prince, Padma Raghavan, Soeb Razzaque, Ben Whelan, and Weikang Zheng.

Appendix A. Effective volume integrals

In a number of examples in the text, a simple population model was applied that assumes a uniform spatial distribution of sources with a fiducial set of source parameters (encapsulated here by the parameter λ). In the case where $z \ll 1$, we can define an effective volume $V^{(\mathrm{eff})}$ for a specific set of trigger conditions by the Euclidean volume integral,

$$\frac{dV^{(\mathrm{eff})}}{d\Omega} = \frac{1}{4\pi}\int_0^D 4\pi r^2 dr P(\mathrm{true}|\lambda, r), \tag{A.1}$$

where $P(\mathrm{true}|r,\lambda)$ is the conditional probability of a true positive detection, given the fiducial source parameters and distance to the source r. The maximum distance D may represent either a physical limitation of the method or else a parameter that we use to regulate the integral before taking $D \to \infty$. The parameter(s) λ may depend on pointing direction, and so we have written $V^{(\mathrm{eff})}$ as differential with respect to solid angle Ω. The expected rate of source detections is then given, after integrating over solid angle, by

$$R = \rho V^{(\mathrm{eff})}, \tag{A.2}$$

where ρ is the intrinsic rate per unit volume of transient sources. In the special case where the observatory is equally sensitive across its field of view, $\frac{dV^{(\mathrm{eff})}}{d\Omega}$ is independent of pointing and we can write

$$R = \rho\Omega\frac{dV^{(\mathrm{eff})}}{d\Omega}. \tag{A.3}$$

In the case where the participating observatories are each monitoring for Poisson processes, P can be taken to be the cumulative Poisson probability distribution above some set of number thresholds $\vec{n}_0$. The vector notation includes the possibility of studying events from multiple observatories, with indices $a = 1 \to M$, so that

$$P(\vec{n} \geqslant \vec{n}_0|\vec{\lambda}, r) = \prod_{a=1}^{M}\left(1 - \sum_{k_a=0}^{n_{0a}}\frac{e^{-\lambda_a/r^2}}{k_a!}\left(\frac{\lambda_a}{r^2}\right)^{k_a}\right), \tag{A.4}$$

where $\lambda_a \equiv \frac{1}{4\pi}\int dE \frac{dN_a}{dE} A_a^{(\mathrm{eff})}(E)$ is a measure of the number of particles that can be detected by observatory a (where N_a is the total number of particles produced and $A_a^{(\mathrm{eff})}$ is the observatory's effective area). It is normalized in such a way that λ_a/r^2 is the expected number of detections for a source at a distance r. The trigger condition $\vec{n} \geqslant \vec{n}_0$ is shorthand for simultaneous detections above the specified number threshold for each observatory.

As such, we are interested in integrals of the form

$$\begin{aligned}\nu_{\vec{k}}(\vec{\lambda}) &\equiv \int_0^D r^2 dr \prod_{a=1}^{M}\frac{e^{-\lambda_a/r^2}}{k_a!}\left(\frac{\lambda_a}{r^2}\right)^{k_a} \\ &= \left(\prod_{a=1}^{M}\frac{\lambda_a^{k_a}}{k_a!}\right)\int_{\Lambda/D^2}^{\infty} dx \frac{\Lambda^{\frac{3}{2}} e^{-x} x^{\kappa-\frac{5}{2}}}{2\Lambda^{\kappa}} \\ &= \frac{\Lambda^{\frac{3}{2}}}{2\kappa!} Q_{\vec{k}}(\vec{\lambda})\Gamma\left(\kappa - \frac{3}{2}, \frac{\Lambda}{D^2}\right),\end{aligned} \tag{A.5}$$

where we have changed the integration variable to $x = \Lambda/r^2$ and defined $\Lambda = \sum_a \lambda_a$, $\kappa = \sum_a k_a$, and the term $Q_{\vec{k}}(\vec{\lambda}) = \left(\frac{\kappa}{k_1, k_2, \ldots}\right)\prod_a \left(\frac{\lambda_a}{\Lambda}\right)^{k_a}$. By the multinomial theorem, we note that

$$\nu_\kappa(\Lambda) \equiv \sum_{\sum k_a = \kappa} \nu_{\vec{k}}(\vec{\lambda}) = \frac{\Lambda^{\frac{3}{2}}}{2\kappa!}\Gamma\left(\kappa - \frac{3}{2}, \frac{\Lambda}{D^2}\right), \tag{A.6}$$

where we have used a single subscript on the left hand side (rather than a vector). As expected, this is the same result as Eq. A.5 applied to a single observatory. The interpretation is that Eq. A.6 can be applied to triggers from multiple observatories that are interchangeable (e.g., when considering $\kappa = 2$ neutrinos form IceCube or ANTARES, regardless of which of the observatories triggered).

Importantly, ν_0 and ν_1 diverge as $D \to \infty$, but the linear combination $\frac{D^3}{3} - \nu_0 - \nu_1$ is finite. Thus, if we are looking for a single Poisson trigger, then a physical limit D must be applied to achieve a finite result (e.g., by requiring that a single detected neutrino orig-

inate from within the sensing region of a gravitational wave network). However, if we instead require that $\kappa \geqslant 2$, then the result is finite as $D \to \infty$.

We can also marginalize over one observatory, defining $\vec{k} = (k_1, \vec{k}')$ and using the normalization of the Poisson series to find

$$\sum_{k_1=0}^{\infty} v_{(k_1,\vec{k}')}(\lambda_1, \vec{\lambda}') = v_{\vec{k}'}(\vec{\lambda}'). \tag{A.7}$$

We can apply this result to two observatories. In the case where we search for at least m events from the first observatory and at least n events from the second,

$$\begin{aligned}\frac{dV_{mn}^{(\mathrm{eff})}}{d\Omega} &= \frac{D^3}{3} - \sum_{i,j \geqslant m,n} v_{(i,j)}(\lambda_1, \lambda_2) \\ &= \frac{D^3}{3} - \sum_{i=0}^{m-1} v_i(\lambda_1) - \sum_{j=0}^{n-1} v_j(\lambda_2) + \sum_{i=0}^{m-1}\sum_{j=0}^{n-1} v_{(i,j)}(\lambda_1, \lambda_2).\end{aligned} \tag{A.8}$$

However, if we search for a total of n events, regardless of which observatory they come from,

$$\frac{dV_{n}^{(\mathrm{eff})}}{d\Omega} = \frac{D^3}{3} - \sum_{j=0}^{n-1} v_j(\Lambda). \tag{A.9}$$

Both Eqs. A.8 and A.9 lead to finite results as $D \to \infty$.

We may wish to consider the case where one or both observatories have an effective area that changes significantly off-axis, meaning that $\frac{dV^{(\mathrm{eff})}}{d\Omega}$ depends on direction. In general, one must carry out the integration over solid angle numerically, although we have already noted the trivial analytic result in the case of Eq. A.3. In addition, there is an analytic solution in the case where only the first observatory has a dependence on zenith angle θ_z, that dependence is proportional to $\cos\theta_z$, and the number threshold of the first observatory is $n_1 \geqslant 1$. However, the result is sufficiently complicated that we choose to omit it here.

Appendix B. Primordial black hole source model

Here we describe the main decay chains leading to the final particle spectra from the PBH explosion under the assumptions of the Standard Model (SM) and Supersymmetry (SUSY).

B.1. SM decay chains

During the final stage of the PBH life, all of the 118 SM particle degrees of freedom (*dof*) are radiated away. Since there are more *dof* for quark and gluons (72) than for leptons and photons (26), the final spectra of both HE and UHE gamma rays and neutrinos originate mostly from the decaying hadrons [104]. Neutrons and antineutrons are produced from these decaying quark fragmentation products, as well.

We assumed that quark and gluon jets emitted during the final stage of PBH evaporation fragment into pions (π^0, π^- and π^+) and baryons ($p, \bar{p}, n$, and $\bar{n}$) with branching ratios of 0.97 and 0.03 [112], respectively. A fragmentation function $\frac{dN_X}{dx}$ of quarks or gluons into a particle of type X has a form [112]:

$$\frac{dN_X}{dx} = \frac{15}{16} x^{-1.5}(1-x)^2, \tag{A.10}$$

where $x = E_X/E, E_X$ is the energy of a particle of type X, and E is the quark/gluon jet energy.

For baryon spectra, we assumed that equal numbers of $p, \bar{p}, n$, and $\bar{n}$ are produced after hadronization. Thus, the final n+$\bar{n}$ spectrum is obtained by multiplying distribution $\frac{dN_X}{dx}$ by 0.015, convolving it with the Hawking primary spectra for quarks and gluons and integrating over time.

The photon spectrum is obtained by convolving a flat photon energy distribution from π^0 decay with the $2 \cdot 1/3 \cdot 0.97 \cdot \frac{dN_X}{dx}$ (where factor 2 accounts for the number of photons produced from each decaying pion and 1/3 is a fraction of neutral pions to the total number of pions) and the Hawking primary spectra.

From decaying π^- and $\pi^+, \bar{\nu}_\mu$ and ν_μ are produced, together with μ^- and μ^+. These neutrinos have flat energy distribution, but there are also secondary neutrinos originating from the consecutive muon decays: $\mu^{+(-)} \to e^{+(-)} + \nu_e(\bar{\nu}_e) + \bar{\nu}_\mu(\nu_\mu)$. Energy distributions of each of these neutrinos are convolved with $2/3 \cdot 0.97 \cdot \frac{dN_X}{dx}$ and the quark/gluon Hawking spectra, and summed afterwards. Since production of ν_τ from decaying hadrons is highly suppressed, most of this neutrino flavor originate from the direct Hawking radiation and from the decays of the directly emitted τ leptons. Therefore, one would expect a flux of ν_τ that is almost two orders of magnitude lower than the total flux of other neutrino flavors. We neglected these two ν_τ contributions to the total neutrino flux in this work.

B.2. SUSY decay chains

If the Minimal Supersymmetric Standard Model (MSSM) describes Nature at the high-energy scales associated with the explosions of PBHs, the number of *dof* available to be radiated increases by more than a factor of two: 244 compared to 118 *dof* in the SM, where we neglected graviton and gravitino *dof* and included five physical Higgs fields (see, for example, Ref. [113]). This leads to an increase of the factor $\alpha(M)$ that directly affects the rate of evaporation by a factor of $\sim$3.3 when the PBH temperature reaches the SUSY particle production energy scale. From that point, the time left until complete evaporation will be shorter compared to the time predicted under the SM assumption. For example, one second before complete evaporation, the temperature of the MSSM PBH would be $T \sim 5.5$ TeV with almost 50% more mass to be radiated than in the case of the SM PBH with $T \sim 8$ TeV at the same time left before its complete evaporation.

Given a number of unknown supersymmetric parameters (more than 100), for simplicity, we assumed that gluinos ($\tilde{g}$) are heavier than squarks ($\tilde{q}$) (as in, for example, the SPS1a benchmark scenario [114] and the mSUGRA B benchmark model [115]), thus they decay into antisquark/quark and squark/antiquark pairs [116]:

$$\tilde{g} \to \bar{\tilde{q}} + q, \tilde{q} + \bar{q}. \tag{A.11}$$

The right chiral states of squarks would decay then mostly into the lightest netralino ($\tilde{\chi}_1^0$):

$$\tilde{q}_R \to \tilde{\chi}_1^0 + q, \tag{A.12}$$

whereas the left handed states would decay into charginos ($\tilde{\chi}_1^\pm$) or heavier neutralinos ($\tilde{\chi}_2^0$) [117]:

$$\tilde{q}_L \to \tilde{\chi}_1^\pm + q, \quad \tilde{\chi}_2^0 + q. \tag{A.13}$$

Further down these decay chains, we assumed that $\tilde{\chi}_1^\pm$ and $\tilde{\chi}_2^0$ preferably decay into leptons and charged leptons plus the lightest neutralino, respectively:

$$\tilde{\chi}_1^\pm \to l^\pm \nu, \quad \tilde{\chi}_2^0 \to l^+ l^- \tilde{\chi}_1^0. \tag{A.14}$$

Without carrying a complete calculation, our rough estimate for the multimessenger particle fluxes under the assumption of the MSSM are: $\sim$4 of the SM flux for neutrinos and $\sim$3.5 of the SM flux for photons and neutrons/antineutrons.

References

[1] G.M. Harry, LIGO Scientific Collaboration, Classical Quantum Gravity 27 (2010) 084006.

[2] F. Acernese, P. Amico, M. Alshourbagy, F. Antonucci, S. Aoudia, S. Avino, D. Babusci, G. Ballardin, F. Barone, L. Barsotti, et al., Classical Quantum Gravity 23 (2006) 635.
[3] M. Ageron, J.A. Aguilar, I. Al Samarai, A. Albert, F. Ameli, M. André, M. Anghinolfi, G. Anton, S. Anvar, M. Ardid, et al., Nucl. Instrum. Methods Phys. Res. A 656 (2011) 11. <arXiv:1104.1607>.
[4] F. Halzen, S.R. Klein, Rev. Sci. Instrum. 81 (2010) 081101. <arXiv:1007.1247>.
[5] J. Abraham, P. Abreu, M. Aglietta, E.J. Ahn, D. Allard, I. Allekotte, J. Allen, J. Alvarez-Muñiz, M. Ambrosio, L. Anchordoqui, et al., Nucl. Instrum. Methods Phys. Res. A 613 (2010) 29. <arXiv:1111.6764>.
[6] N. Gehrels, G. Chincarini, P. Giommi, K.O. Mason, J.A. Nousek, A.A. Wells, N.E. White, S.D. Barthelmy, D.N. Burrows, L.R. Cominsky, et al., Astrophys. J. 611 (2004) 1005.
[7] M. Ackermann, M. Ajello, A. Albert, A. Allafort, W.B. Atwood, M. Axelsson, L. Baldini, J. Ballet, G. Barbiellini, D. Bastieri, et al., Astrophys. J. Suppl. 203 (2012) 4. <arXiv:1206.1896>.
[8] F. Aharonian, A.G. Akhperjanian, A.R. Bazer-Bachi, M. Beilicke, W. Benbow, D. Berge, K. Bernlöhr, C. Boisson, O. Bolz, V. Borrel, et al., Astron. Astrophys. 457 (2006) 899. <arXiv:astro-ph/0607333>.
[9] J. Holder, E. Aliu, T. Arlen, T. Aune, M. Beilicke, W. Benbow, M. Bottcher, A. Bouvier, J. H. Buckley, V. Bugaev, et al., ArXiv e-prints (2011) <arXiv:1111.1225>.
[10] J. Cortina, F. Goebel, T. Schweizer, and for the MAGIC Collaboration, ArXiv e-prints (2009) <arXiv:0907.1211>.
[11] A. Tepe, and the Hawc Collaboration, J. Phys. Conf. Ser. 375 (2012) 052026.
[12] C.W. Akerlof, R.L. Kehoe, T.A. McKay, E.S. Rykoff, D.A. Smith, D.E. Casperson, K.E. McGowan, W.T. Vestrand, P.R. Wozniak, J.A. Wren, et al., Pub. Astr. Soc. Pacific 115 (2003) 132. <arXiv:astro-ph/0210238>.
[13] N.M. Law, S.R. Kulkarni, R.G. Dekany, E.O. Ofek, R.M. Quimby, P.E. Nugent, J. Surace, C.C. Grillmair, J.S. Bloom, M.M. Kasliwal, et al., Pub. Astr. Soc. Pacific 121 (2009) 1395. <arXiv:0906:5350>.
[14] N. Gehrels, E. Ramirez-Ruiz, D.B. Fox, Annu. Rev. Astron. Astrophys. 47 (2009) 567. <arXiv:0909.1531>.
[15] A.I. MacFadyen, S.E. Woosley, Astrophys. J. 524 (1999) 262. <arXiv:astro-ph/9810274>.
[16] S.E. Woosley, J.S. Bloom, Ann. Rev. Astron. Astrophys. 44 (2006) 507. <arXiv:astro-ph/0609142>.
[17] S.B. Cenko, D.A. Frail, F.A. Harrison, J.B. Haislip, D.E. Reichart, N.R. Butler, B.E. Cobb, A. Cucchiara, E. Berger, J.S. Bloom, et al., Astrophys. J. 732 (2011) 29. <arXiv:1004.2900>.
[18] P. Mészáros, Rep. Prog. Phys. 69 (2006) 2259. <arXiv:astro-ph/0605208>.
[19] P. Mészáros, ArXiv e-prints (2012) <arXiv:1204.1897>.
[20] E. Waxman, J. Bahcall, Phys. Rev. Lett. 78 (1997) 2292. <arXiv:astro-ph/9701231>.
[21] J.P. Rachen, P. Mészáros, Phys. Rev. D 58 (1998) 123005. <arXiv:astro-ph/9802280>.
[22] D. Guetta, D. Hooper, J. Alvarez-MunÎz, F. Halzen, E. Reuveni, Astropart. Phys. 20 (2004) 429. <arXiv:astro-ph/0302524>.
[23] R. Abbasi, Y. Abdou, T. Abu-Zayyad, J. Adams, J.A. Aguilar, M. Ahlers, K. Andeen, J. Auffenberg, X. Bai, M. Baker, et al., Phys. Rev. Lett. 106 (2011) 141101. <arXiv:1101.1448>.
[24] R. Abbasi, Y. Abdou, T. Abu-Zayyad, J. Adams, J.A. Aguilar, M. Ahlers, D. Altmann, K. Andeen, J. Auffenberg, X. Bai, et al., Phys. Rev. D 84 (2011) 082001. <arXiv:1104.5187>.
[25] M. Ahlers, M.C. Gonzalez-Garcia, F. Halzen, Astropart. Phys. 35 (2011) 87. <arXiv:1103.3421>.
[26] S. Hümmer, P. Baerwald, W. Winter, ArXiv e-prints (2011), <arXiv:1112.1076>.
[27] Z. Li, Phys. Rev. D 85 (2012) 027301. <arXiv:1112.2240>.
[28] H.-N. He, R.-Y. Liu, X.-Y. Wang, S. Nagataki, K. Murase, Z.-G. Dai, ArXiv e-prints (2012), <arXiv:1204.0857>.
[29] S. Kobayashi, P. Mészáros, Astrophys. J. 589 (2003) 861. <arXiv:astro-ph/0210211>.
[30] C.D. Ott, C. Reisswig, E. Schnetter, E. O'Connor, U. Sperhake, F. Löffler, P. Diener, E. Abdikamalov, I. Hawke, A. Burrows, Phys. Rev. Lett. 106 (2011) 161103. <arXiv:1012.1853>.
[31] A. Corsi, P. Mészáros, Astrophys. J. 702 (2009) 1171. <arXiv:0907.2290>.
[32] K. Kiuchi, M. Shibata, P.J. Montero, J.A. Font, Phys. Rev. Lett. 106 (2011) 251102. <arXiv:1105.5035>.
[33] A.M. Soderberg, S.R. Kulkarni, E. Nakar, E. Berger, P.B. Cameron, D.B. Fox, D. Frail, A. Gal-Yam, R. Sari, S.B. Cenko, et al., Nature 442 (2006) 1014. <arXiv:astro-ph/0604389>.
[34] D. Guetta, M. Della Valle, Astrophys. J. Lett. 657 (2007) L73. <arXiv:astro-ph/0612194>.
[35] E. Liang, B. Zhang, F. Virgili, Z.G. Dai, Astrophys. J. 662 (2007) 1111, <arXiv:astro-ph/0605200>.
[36] A.M. Soderberg, S. Chakraborti, G. Pignata, R.A. Chevalier, P. Chandra, A. Ray, M.H. Wieringa, A. Copete, V. Chaplin, V. Connaughton, et al., Nature 463 (2010) 513. <arXiv:0908.2817>.
[37] B. Katz, R. Budnik, E. Waxman, Astrophys. J. 716 (2010) 781. <arXiv:0902.4708>.
[38] E. Nakar, R. Sari, Astrophys. J. 747 (2012) 88. <arXiv:1106.2556>.
[39] K. Murase, K. Ioka, S. Nagataki, T. Nakamura, Astrophys. J. Lett. 651 (2006) L5. <arXiv:astro-ph/0607104>.
[40] N. Gupta, B. Zhang, Astropart. Phys. 27 (2007) 386. <arXiv:astro-ph/0606744>.
[41] K. Kashiyama, K. Murase, S. Horiuchi, S. Gao, P. Mészáros (2012), <arXiv:1210.8147>.
[42] J.P. Norris, J.T. Bonnell, Astrophys. J. 643 (2006) 266. <arXiv:astro-ph/0601190>.
[43] E. Nakar, Phys. Rep. 442 (2007) 166. <arXiv:astro-ph/0701748>.
[44] V. Kalogera, C. Kim, D.R. Lorimer, M. Burgay, N. D'Amico, A. Possenti, R.N. Manchester, A.G. Lyne, B.C. Joshi, M.A. McLaughlin, et al., Astrophys. J. Lett. 601 (2004) L179.
[45] W. Fong, E. Berger, R. Margutti, B.A. Zauderer, E. Troja, I. Czekala, R. Chornock, N. Gehrels, T. Sakamoto, D.B. Fox, et al., Astrophys. J. 756 (2012) 189. <arXiv:1204.5475>.
[46] P. Mészáros, E. Waxman, Phys. Rev. Lett. 87 (2001) 171102. <arXiv:astro-ph/0103275>.
[47] S. Razzaque, P. Mészáros, E. Waxman, Phys. Rev. D 68 (2003) 083001. <arXiv:astro-ph/0303505>.
[48] S. Horiuchi, S. Ando, Phys. Rev. D 77 (2008) 063007. <arXiv:0711.2580>.
[49] W. Zhang, S.E. Woosley, A. Heger, Astrophys. J. 608 (2004) 365, <arXiv:astro-ph/0308389>.
[50] W.D. Arnett, J.N. Bahcall, R.P. Kirshner, S.E. Woosley, Ann. Rev. Astron. Astrophys. 27 (1989) 629.
[51] A.M. Soderberg, E. Berger, K.L. Page, P. Schady, J. Parrent, D. Pooley, X.-Y. Wang, E.O. Ofek, A. Cucchiara, A. Rau, et al., Nature 453 (2008) 469. <arXiv:0802.1712>.
[52] R. Abbasi, Y. Abdou, T. Abu-Zayyad, M. Ackermann, J. Adams, J.A. Aguilar, M. Ahlers, M.M. Allen, D. Altmann, K. Andeen, et al., Astron. Astrophys. 535 (2011) A109.
[53] E.O. Ofek, D. Fox, S.B. Cenko, M. Sullivan, O. Gnat, D.A. Frail, A. Horesh, A. Corsi, R.M. Quimby, N. Gehrels, et al., ArXiv e-prints (2012), <arXiv:1206.0748>.
[54] C. Reisswig, C.D. Ott, U. Sperhake, E. Schnetter, Phys. Rev. D 83 (2011) 064008. <arXiv:1012.0595>.
[55] A.M. Hillas, ArXiv Astrophysics e-prints (2006), <arXiv:astro-ph/0607109>.
[56] The Pierre Auger Collaboration, P. Abreu, M. Aglietta, E.J. Ahn, I.F.M. Albuquerque, D. Allard, I. Allekotte, J. Allen, P. Allison, J. Alvarez Castillo, et al., ArXiv e-prints (2011), <arXiv:1107.4805>.
[57] A. Atoyan, C.D. Dermer, Phys. Rev. Lett. 87 (2001) 221102, <arXiv:astro-ph/0108053>.
[58] A.Mücke, R.J. Protheroe, R. Engel, J.P. Rachen, T. Stanev, Astropart. Phys. 18 (2003) 593, <arXiv:astro-ph/0206164>.
[59] A.A. Abdo, M. Ackermann, I. Agudo, M. Ajello, H.D. Aller, M.F. Aller, E. Angelakis, A.A. Arkharov, M. Axelsson, U. Bach, et al., Astrophys.J. 716 (2010) 30. <arXiv:0912.2040>.
[60] J. Poutanen, B. Stern, Astrophys. J. Lett. 717 (2010) L118. <arXiv:1005.3792>.
[61] M. Boettcher, ArXiv e-prints (2010). <arXiv:1006.5048>.
[62] J. Holder, I.H. Bond, P.J. Boyle, S.M. Bradbury, J.H. Buckley, D.A. Carter-Lewis, W. Cui, C. Dowdall, C. Duke, I. de la Calle Perez, et al., Astrophys. J. Lett. 583 (2003) L9, <arXiv:astro-ph/0212170>.
[63] H. Krawczynski, S.B. Hughes, D. Horan, F. Aharonian, M.F. Aller, H. Aller, P. Boltwood, J. Buckley, P. Coppi, G. Fossati, et al., Astrophys. J. 601 (2004) 151, <arXiv:astro-ph/0310158>.
[64] F. Halzen, D. Hooper, Astropart. Phys. 23 (2005) 537, <arXiv:astro-ph/0502449>.
[65] S.W. Hawking, Nature 248 (1974) 30.
[66] D.N. Page, Phys. Rev. D 13 (1976) 198.
[67] J.H. MacGibbon, B.R. Webber, Phys. Rev. D 41 (1990) 3052.
[68] Y.B. Zel'dovich, I.D. Novikov, Soviet Ast. 10 (1967) 602.
[69] S. Hawking, M.N.R.A.S 152 (1971) 75.
[70] C.T. Hill, Nucl. Phys. B 224 (1983) 469.
[71] R.J. Protheroe, P.A. Johnson, Astropart. Phys. 4 (1996) 253, <arXiv:astro-ph/9506119>.
[72] V. Berezinsky, M. Kachelrieß, A. Vilenkin, Phys. Rev. Lett. 79 (1997) 4302, <arXiv:astro-ph/9708217>.
[73] V. Berezinsky, P. Blasi, A. Vilenkin, Phys. Rev. D 58 (1998) 103515, <arXiv:astro-ph/9803271>.
[74] S. Sarkar, R. Toldrà, Nucl. Phys. B 621 (2002) 495, <arXiv:hep-ph/0108098>.
[75] R. Aloisio, V. Berezinsky, M. Kachelrieß, Phys. Rev. D 74 (2006) 023516, <arXiv:astro-ph/0604311>.
[76] J. Ellis, V.E. Mayes, D.V. Nanopoulos, Phys. Rev. D 74 (2006) 115003, <arXiv:astro-ph/0512303>.
[77] S.D. Barthelmy, P. Butterworth, T.L. Cline, N. Gehrels, F. Marshall, T. Takeshima, V. Connaughton, R.M. Kippen, C. Kouveliotou, C.R. Robinson, in: C.A. Meegan, R.D. Preece, T.M. Koshut (Eds.), Gamma-Ray Bursts, 4th Hunstville Symposium, American Institute of Physics Conference Series, vol. 428, 1998, pp. 99–103.
[78] R. Abbasi, Y. Abdou, T. Abu-Zayyad, M. Ackermann, J. Adams, J.A. Aguilar, M. Ahlers, M.M. Allen, D. Altmann, K. Andeen, et al., Astron. Astrophys. 539 (2012) A60. <arXiv:1111.7030>.
[79] P.A. Evans, J.K. Fridriksson, N. Gehrels, J. Homan, J.P. Osborne, M. Siegel, A. Beardmore, P. Handbauer, J. Gelbord, J.A. Kennea, et al., ArXiv e-prints (2012), <arXiv:1205.1124>.
[80] A. Homeier, in: International Cosmic Ray Conference, International Cosmic Ray Conference, vol. 4, 2011, p. 185.
[81] R. Abbasi et al., Astrophys. J. 701 (2009) 1721, <http://stacks.iop.org/0004-637X/701/i=2/a=1721>.
[82] J. Braun, M. Baker, J. Dumm, C. Finley, A. Karle, T. Montaruli, Astropart. Phys. 33 (2010) 175, ISSN 0927-6505, <http://www.sciencedirect.com/science/article/pii/S0927650510000241>.

[83] B. Abbott, R. Abbott, R. Adhikari, J. Agresti, P. Ajith, B. Allen, R. Amin, S.B. Anderson, W.G. Anderson, M. Arain, et al., Phys. Rev. D 77 (2008) 062004. <arXiv:0709.0766>.
[84] B.P. Abbott, R. Abbott, F. Acernese, R. Adhikari, P. Ajith, B. Allen, G. Allen, M. Alshourbagy, R.S. Amin, S.B. Anderson, et al., Astrophys. J. 715 (2010) 1438. <arXiv:0908.3824>.
[85] B. Abbott, R. Abbott, R. Adhikari, J. Agresti, P. Ajith, B. Allen, R. Amin, S.B. Anderson, W.G. Anderson, M. Arain, et al., Phys. Rev. D 76 (2007) 062003. <arXiv:astro-ph/0703419>.
[86] The LIGO Scientific Collaboration, Phys. Rev. Lett. 101 (2008) 211102, p. 6.
[87] J. Abadie, B.P. Abbott, R. Abbott, M. Abernathy, T. Accadia, F. Acernese, C. Adams, R. Adhikari, C. Affeldt, B. Allen, et al., Astrophys. J. Lett. 734 (2011) L35+. <arXiv:1011.4079>.
[88] B.P. Abbott, R. Abbott, M. Abernathy, T. Accadia, et al. (2011), <arXiv:1109.3498v1>.
[89] S.D. Barthelmy, L.M. Barbier, J.R. Cummings, E.E. Fenimore, N. Gehrels, D. Hullinger, H.A. Krimm, C.B. Markwardt, D.M. Palmer, A. Parsons, et al., Space Sci. Rev. 120 (2005) 143, <arXiv:astro-ph/0507410>.
[90] A.A. Abdo, M. Ackermann, M. Ajello, A. Allafort, E. Antolini, W.B. Atwood, M. Axelsson, L. Baldini, J. Ballet, G. Barbiellini, et al., Astrophys. J. Suppl. Series 188 (2010) 405, <http://stacks.iop.org/0067-0049/188/i=2/a=405>.
[91] <http://amon.gravity.psu.edu/mou.shtml>.
[92] A. Franckowiak, C. Akerlof, D.F. Cowen, M. Kowalski, R. Lehmann, T. Schmidt, F. Yuan, Tech. Rep. (2009), in: Proceedings of the 31st ICRC, Lodz, Poland, July 2009, p. 4, 2 figures, <arXiv:0909.0631>.
[93] The IceCube Collaboration, ArXiv e-prints (2011) <arXiv:1111.2741>.
[94] B. Abbott, R. Abbott, R. Adhikari, P. Ajith, B. Allen, G. Allen, R. Amin, S.B. Anderson, W.G. Anderson, M.A. Arain, et al., Classical Quantum Gravity 25 (2008) 114051. <arXiv:0802.4320>.
[95] LIGO Scientific Collaboration, Virgo Collaboration, J. Abadie, B.P. Abbott, R. Abbott, T.D. Abbott, M. Abernathy, T. Accadia, F. Acernese, C. Adams, et al., Astron. Astrophys. 539 (2012) A124, <arXiv:1109.3498>.
[96] J. Abadie, B.P. Abbott, R. Abbott, M. Abernathy, T. Accadia, F. Acernese, C. Adams, R. Adhikari, P. Ajith, B. Allen, et al., Classical Quantum Gravity 27 (2010) 173001. <arXiv:1003.2480>.
[97] I. Bartos, C. Finley, A. Corsi, S. Márka, Phys. Rev. Lett. 107 (2011) 251101. <arXiv:1108.3001>.
[98] B. Baret, I. Bartos, B. Bouhou, E. Chassande-Mottin, A. Corsi, I. Di Palma, C. Donzaud, M. Drago, C. Finley, G. Jones, et al., J. Phys. Conf. Ser. 363 (2012) 012022.
[99] Y. Aso, Z. Márka, C. Finley, J. Dwyer, K. Kotake, S. Márka, Classical Quantum Gravity 25 (2008) 114039. <arXiv:0711.0107>.
[100] The ANTARES Collaboration, the LIGO Scientific Collaboration, the Virgo Collaboration, S. Adrián-Martínez, I.A. Samarai, A. Albert, M. André, M. Anghinolfi, G. Anton, S. Anvar, et al., ArXiv e-prints (2012) <arXiv:1205.3018>.
[101] J. Abadie, B.P. Abbott, R. Abbott, T. Accadia, F. Acernese, R. Adhikari, P. Ajith, B. Allen, G. Allen, E. Amador Ceron, et al., Phys. Rev. D 81 (2010) 102001. <arXiv:1002.1036>.
[102] H.-Y. Chen, D.E. Holz, ArXiv e-prints (2012), <arXiv:1206.0703>.
[103] R. Abbasi, Y. Abdou, T. Abu-Zayyad, M. Ackermann, J. Adams, J.A. Aguilar, M. Ahlers, D. Altmann, K. Andeen, J. Auffenberg, et al., Nature 484 (2012) 351. <arXiv:1204.4219>.
[104] J.H. MacGibbon, B.R. Webber, Phys. Rev. D 41 (1990) 3052.
[105] A.F. Heckler, Phys. Rev. Lett. 78 (1997) 3430, <arXiv:astro-ph/9702027>.
[106] R. Daghigh and J. Kapusta, Phys. Rev. D 65 (2002) 064028, <arXiv:gr-qc/0109090>.
[107] F. Halzen, E. Zas, J.H. MacGibbon, T.C. Weekes, Nature 353 (1991) 807.
[108] J.H. MacGibbon, Phys. Rev. D 44 (1991) 376.
[109] F. Halzen, B. Keszthelyi, E. Zas, Phys. Rev. D 52 (1995) 3239, <arXiv:hep-ph/9502268>.
[110] A.U. Abeysekara, J.A. Aguilar, S. Aguilar, R. Alfaro, E. Almaraz, C. Álvarez, J.d.D. Álvarez-Romero, M. Álvarez, R. Arceo, J.C. Arteaga-Velázquez, et al., Astropart. Phys. 35 (2012) 641. <arXiv:1108.6034>.
[111] G. Tešić, Veritas Collaboration, J. Phys. Conf. Ser. 375 (2012) 052024.
[112] C.T. Hill, D.N. Schramm, T.P. Walker, Phys. Rev. D 36 (1987) 1007.
[113] G. Jungman, M. Kamionkowski, K. Griest, Phys. Rep. 267 (1996) 195, <arXiv:hep-ph/9506380>.
[114] B.C. Allanach, M. Battaglia, G.A. Blair, M. Carena, A. de Roeck, A. Dedes, A. Djouadi, D. Gerdes, N. Ghodbane, J. Gunion, et al., Eur. Phys. J. C 25 (2002) 113, <arXiv:hep-ph/0202233>.
[115] J. Ellis, J.L. Feng, A. Ferstl, K.T. Matchev, K.A. Olive, Eur. Phys. J. C 24 (2002) 311, <arXiv:astro-ph/0110225>.
[116] W. Beenakker, R. Höpker, P.M. Zerwas, Phys. Lett. B 378 (1996) 159, <arXiv:hep-ph/9602378>.
[117] M. Krämer, E. Popenda, M. Spira, P.M. Zerwas, Phys. Rev. D 80 (2009) 055002. <arXiv:0902.3795>.